The Texas A&M University

Department of Physics

College Station, Texas 77843

Report No. 4

Degree and Plane of Polarization of Multiple Scattered Light

II. Earth's Atmosphere with Aerosols

By Gilbert N. Plass and George W. Kattawar

Date of Issue: April 1, 1972

Grant No. NGR 44-001-117

Principal Investigators: Gilbert N. Plass

George W. Kattawar

Degree and Plane of Polarization of Multiple Scattered Light

II. Earth's Atmosphere with Aerosols

Gilbert N. Plass and George W. Kattawar

Department of Physics, Texas A&M University, College Station, Texas 77843

ABSTRACT

The degree of polarization as well as the direction of the plane of polarization are calculated by a Monte Carlo method for the reflected and transmitted photons from the earth's atmosphere. The solar photons are followed through multiple collisions with the aerosols and the Rayleigh scattering centers in the atmosphere. The aerosol number density as well as the ratio of aerosol to Rayleigh scattering varies with height. The proportion of aerosol to Rayleigh scattering is appropriately chosen at each wavelength (λ = 0.4μ and 0.7μ); ozone absorption is included where appropriate. Three different aerosol number densities are used to study the effects of aerosol variations. Results are given for a solar zenith angle of 81.37^{o} and a surface albedo of zero. The polarization of the reflected and transmitted photons is particularly sensitive to the amount of aerosols in the atmosphere at certain angles of observation.

Introduction

Among the factors which influence the degree of polarization of the solar radiation scattered within the earth's atmosphere are the solar angle, the angle of observation, the wavelength, the characteristics of the boundary, and the aerosol number density and distribution with height together with the appropriate single scattering function. Results of polarization calculations for models which attempt to incorporate most of these features have only been obtained to date by Monte Carlo methods [1, 2, 3], although other methods are being developed which should be capable of solving this problem.

The Monte Carlo method used here is described in the first part of this paper[4] (referred to hereafter as I). In this method the scattering angles are chosen from the exact angular aerosol scattering function with a strong forward peak, as calculated from Mie theory. The aerosol concentrations may vary in any desired manner with height. The results include all orders of scattering. The polarization previously presented by Plass and Kattawar[1] is calculated from the Rubenson definition (Eq. (1) of I). In this paper the polarization is calculated from the four components of the Stokes vector (Eq. (2) of I), which together with the angle of the plane of polarization specifies the polarization state.

Method

The aerosols are represented by particles with a real index of refraction of 1.55 and with radii proportional to r^{-4}. The scattering matrix for this distribution of spherical particles was calculated exactly from the Mie theory[5] for the wavelengths used in this calculation. The single scattering function obtained is similar to the one shown in Fig. 1 of Ref. 2 and the single scattered polarization to that shown in Fig. 1 of Ref. 1. All four of the independent components of the scattering matrix were calculated as input data for the Monte Carlo calculations.

The Rayleigh attenuation coefficient, ozone absorption coefficient, and the aerosol number density as a function of height and wavelength were taken from the tables compiled by Elterman[6]. The total optical thickness of the atmosphere was calculated from the Rayleigh and aerosol attenuation coefficients and the ozone absorption coefficient. The atmosphere was divided into a number of layers, and the ratio of the total scattering to the total extinction coefficient as well as the ratio of the Rayleigh scattering to the total scattering extinction coefficient were established for each layer as was the ozone extinction coefficient. All calculations were done with the optical depth as the parameter. A surface albedo equal to zero was assumed for all results reported here. The Monte Carlo code which includes polarization is described in I.

Polarization of Reflected Photons at $\lambda = 0.4\mu$.

The degree of polarization as well as the direction of the plane of polarization of the reflected photons as observed at the top of the atmosphere was calculated at $\lambda = 0.4\mu$. The variation of aerosol concentration with height was taken into account as already described by the calculation of the appropriate ratios of the extinction lengths for each of the atmospheric layers. The normal aerosol distribution is based on the tables of Elterman[6]; the Rayleigh extinction length is greater than the aerosol extinction length at all altitudes above 3 km. The ozone absorption is negligible at this wavelength. A solar zenith angle of 81.37^{o} ($\mu = 0.15$) was chosen for all of the calculations presented here. The variation of the plane of polarization is most interesting when the sun is away from the region of the sky near the zenith.

The polarization of the reflected photons calculated from Eq. (2) of I is shown in Figs. 1 - 3. In each figure the polarization is plotted as a function of the cosine of the nadir angle μ. The results are averaged in each case over a 30^{o}

range in ϕ, the azimuthal angle, measured from the incident plane. For example, in Fig. 1 the solar horizon is on the left, the nadir is at the center, and the antisolar horizon is at the right of the figure.

The polarization of single scattered photons was calculated for five different atmospheric models and the results are shown in each figure. These results were averaged over the indicated range in ϕ so that they could be compared directly with the multiple scattered Monte Carlo results. The first model for single scattering assumes that no aerosols are present in the atmosphere and that all scattering is Rayleigh (crosses—Model R). The second model assumes that only the aerosols given by the Elterman tables[6] are present with no Rayleigh scattering (diamonds—Model A). The third model assumes the normal aerosol amount from the Elterman tables plus Rayleigh scattering (open triangles—Model R + A). The fourth and fifth models assume one-third and three times the normal aerosol amount at each altitude plus Rayleigh scattering (pluses—Model R + $\frac{1}{3}$ A and octagons - Model R + 3 A respectively). When less than five of these symbols appear for a given value of μ, the omitted values are within the width of one symbol of a plotted value. It is clear from a study of the curves where the omitted points are located.

The results of four different Monte Carlo calculations are also shown in each figure. Each value is the average polarization for the photons received over a range of 0.1 in the cosine of the nadir angle μ and a range of 30° in the azimuthal angle. For example, the results just to the left of the nadir in Fig. 1 represent the average polarization over the range $0.9 < \mu < 1.0$ and $0^{\circ} < \phi < 30^{\circ}$. The Monte Carlo results include all orders of multiple scattering which contribute to the polarization. The solid triangles with the point up represent the results for multiple scattering from the normal aerosol distribution as given by the

Elterman tables plus Rayleigh scattering (Model R + A). The results were also calculated for one-third and three times the normal aerosol amount at each altitude plus Rayleigh scattering (solid circles—Model R + $^1/_3$ A and solid triangle with point down-Model R + 3 A respectively). The solid squares give results for a normal aerosol atmosphere plus Rayleigh scattering with in addition a cloud of optical thickness unity at an altitude of 5 km (Model C). A nimbostratus model[7] is assumed for the cloud particles with the particle concentration proportional to r^6 exp (0.5r), where r is the radius of the particle with an index of refraction of 1.33; the modal radius for this distribution is 12μ.

The polarization of the single scattered photons is greater for Model R than for Model A at most angles of observation. The Rayleigh polarization is the largest of the various models in Figs. 1 - 3 except for some nadir angles when $120^o < \phi < 180^o$. As aerosols are added to the Rayleigh atmosphere the polarization decreased in general as the aerosol amount increases. This occurs even at nadir angles where the single scattered polarization is greater for Model A than for Model R; the reason for this variation is connected with the fact that the average height of scattering increases as the nadir angle of observation approaches the horizon and thus the scattering comes from a region high in the atmosphere where the Rayleigh scattering is more important than aerosol scattering.

In most cases in Figs. 1 - 3 the polarization of the multiple scattered photons is less than that from the single scattered photons for the corresponding model. A notable exception is when $0.0 < \mu < 0.4$ and $150^o < \phi < 180^o$; in this region the polarization of the multiple scattered photons is consistently greater than that for the single scattered photons for the same model. This effect occurs whenever there is a region of high polarization for single scattered photons (near $\mu = 1$ in this case) together with a region of very low polarization (near $\mu = 0$ at both horizons in this case).

The direction of the plane of polarization is shown in Figs. 4 - 6. As pointed out in I, only two values of χ are possible for a given μ and ϕ; these two values differ by 90°. The sign of the element M^{-} from the first row and second column of the Stokes scattering matrix in the I, Q, U, V representation determines which of these two values occurs. The single scattered χ values shown in these figures have been averaged over the indicated 30° range in ϕ. If both signs of M^{-} can occur within this range of ϕ, then the average value of χ may have an intermediate value between the two possible values that can be obtained from an individual measurement.

It is interesting to compare the χ values for single scattered photons in Fig. 4 when $0^{\circ} < \phi < 30^{\circ}$; as μ increases from 0 to 1, χ decreases smoothly from a value of about -28° to -75° at the nadir for Model R, while χ varies rapidly over its entire range for Model A. When $60^{\circ} < \phi < 90^{\circ}$ (Fig. 6), the χ values for Models R and A differ by 90° near $\mu = 0$, since M^{-} has opposite signs for the two models. However, near the nadir the χ value for Model A approaches that for Model R, since M^{-} has the same sign for both models over the range of scattering angles appropriate for this case. When not shown separately, the χ values for Models R + A, R + $\frac{1}{3}$ A, and R + 3 A are the same as those for Model R. The χ values for the multiple scattered photons obtained from the Monte Carlo calculations are reasonably close to those for single scattered photons from Model R in all cases. The Monte Carlo results show little variation between the four cases calculated.

Polarization of Reflected Photons at $\lambda = 0.7\mu$.

The Rayleigh, aerosol, and ozone attenuation coefficients were taken from the tables of Elterman[6]. The aerosol attenuation coefficient is greater than the Rayleigh attenuation coefficient at all altitudes up to 35 km. Ozone absorption is important at this wavelength; the ozone absorption coefficient is larger than

the Rayleigh attenuation coefficient at all altitudes above 20 km which are considered in this calculation.

The polarization for both single and multiple scattered photons is given in Figs. 7 - 9. At most viewing angles the single scattered polarization is less at $\lambda = 0.7\mu$ than at $\lambda = 0.4\mu$ for the three models with various aerosol amounts. The aerosol contribution compared to the Rayleigh is considerably more important at $\lambda = 0.7\mu$ than at 0.4μ. At most scattering angles the single scattered polarization is less from aerosol than from Rayleigh scattering centers. Thus the polarization is usually less at $\lambda = 0.7\mu$ than at 0.4μ. The single scattered polarization for Model A shows differences of detail between the two wavelengths.

The polarization of the multiple scattered photons calculated by the Monte Carlo method shows much larger differences as the aerosol amount is varied from one-third normal to three times normal at $\lambda = 0.7\mu$ than at $\lambda = 0.4\mu$. In almost all cases the polarization decreases as the aerosol amount increases. It is interesting to compare the polarization of the single scattered with the multiple scattered photons for the same model; in almost all cases the Monte Carlo results are less than the corresponding single scattered results. A comparison of these two curves gives an indication of the statistical fluctuation of the Monte Carlo results. The polarization of the reflected photons when there is a $\tau = 1$ cloud in the atmosphere at 5 km (Model C) is shown by the solid squares. This curve is usually below the curve for the atmosphere with the normal aerosol amount.

Appreciable differences in the polarization of the reflected radiation develop as the aerosol amount in the atmosphere varies. For example, near the nadir in the incident plane with $0^\circ < \phi < 30^\circ$, the polarization is 0.56, 0.32, and 0.19 for one-third, normal, and three times normal aerosol amount. Measurements

of the polarization of the reflected radiation taken from the top of the atmosphere at appropriate angles could provide an important indication of the aerosol amount in the atmosphere. Of course, changes in the polarization due to other atmospheric variables would also have to be taken into account.

The plane of polarization is given in Figs. 10 - 12. The curves for single scattered photons are appreciably different in many cases from the results at $\lambda = 0.4\mu$. In most cases the χ values for the multiple scattered photons are nearly the same at both wavelengths. Also in most cases there is very little difference between the χ values for the different models. One striking exception is for $0^o < \phi < 30^o$ where the χ values are quite different for Model C compared to those for the other models. The position of the plane of polarization does not change appreciably as the aerosol amount in the atmosphere changes.

Polarization of Transmitted Photons at $\lambda = 0.4\mu$.

The polarization of the transmitted photons as a function of the cosine of the zenith angle μ is given in Figs. 13 - 15. The solar horizon is on the left of each graph, the zenith is in the center, and the antisolar horizon is on the right. The polarization is very small near the direction of the incoming solar photons in all cases. The maximum value occurs at scattering angles near 90^o for Model R and near the rainbow angle for Model A. The curves for single scattering shown in Figs. 13 - 15 indicate that the polarization decreases as the aerosol amount increases and has the smallest value for Model A except in the incident plane near the antisolar horizon. The polarization of the multiple scattered photons is usually less than that of single scattered photons except in regions where the single scattered polarization is very small; an example of this effect occurs near the solar horizon when $0^o < \phi < 30^o$.

In most cases the polarization is less when there is a $\tau = 1$ nimbostratus cloud at 5 km than when it is absent. In all cases the polarization increases near the horizon as the azimuthal angle ϕ increases from 0^{o} to 90^{o} and then decreases as ϕ increases from 90^{o} to 180^{o}.

The plane of polarization of the transmitted photons is shown in Figs. 16 - 18. The values of χ for single scattered photons are very close together for all models except Model A. In some cases, as for example when $0^{o} < \phi < 30^{o}$, the value of χ is a rapidly varying function of μ that passes through 90^{o} four times as the viewing angle goes from the horizon to the zenith. On the other hand the value of χ changes relatively slowly for the other models over this same range. The χ values for the multiple scattered photons are close to those for the single scattered case for the same model except in the incident plane; in this latter case some deviations are evident both between models and between the single and multiple scattered curves.

Polarization of the Transmitted Photons at $\lambda = 0.7\mu$.

The polarization of the transmitted photons is shown in Figs. 19 - 21. The variation of the polarization with the aerosol content of the atmosphere is more marked at $\lambda = 0.7\mu$ than at 0.4μ, for the same reasons as have been discussed in connection with the reflected photons. There are many angles of observation for ϕ near 90^{o} such that the polarization of the multiple scattered photons varies from around 0.6 for Model R + $\frac{1}{3}$ A to approximately 0.2 for Model R + 3 A. A measurement of the polarization at these angles should be a sensitive indicator of the number of aerosol particles present. It should be pointed out though that other factors such as the composition and size of the aerosols may also influence the observed polarization at these angles.

The variation of the plane of polarization is shown in Figs. 22 - 24. The

value of χ for Model R and the Rayleigh plus aerosol models is nearly the same in most cases. The value for Model A does not show the rapid variation with μ when $0^{o} < \phi < 30^{o}$ that was evident at $\lambda = 0.4\mu$ and also does not deviate from the value for the other four models except when $120^{o} < \phi < 180^{o}$. Except in a few cases the χ values for the multiple scattered photons are quite close to those for the single scattered photons. It would be difficult to determine the aerosol content of the atmosphere from measurement of χ alone. The degree of polarization is much more sensitive to the atmospheric aerosol amount.

This work was supported by Grant No. NGR 44-001-117 from the National Aeronautics and Space Administration.

REFERENCES

1. G. N. Plass and G. W. Kattawar, Appl. Opt. 9, 1122 (1970).

2. G. N. Plass and G. W. Kattawar, Appl. Opt. 7, 1129 (1968).

3. G. N. Plass and G. W. Kattawar, J. Atmosph. Sci. 28, 1187 (1970).

4. G. W. Kattawar and G. N. Plass, Appl. Opt. (submitted, part I of this paper).

5. G. W. Kattawar and G. N. Plass, Appl. Opt. 6, 1377, 1549 (1967).

6. L. Elterman, UV, Visible, and IR Attenuation for Altitudes to 50 km, 1968. Air Force Cambridge Research Laboratories Report AFCRL-68-0153 (1968); appl. Opt. 8, 893 (1969).

7. G. W. Kattawar and G. N. Plass, Appl. Opt. 7, 869 (1968).

CAPTIONS FOR FIGURES

Fig. 1. Polarization of reflected radiation as a function of the cosine of the nadir angle μ for $\lambda = 0.4\mu$. The cosine of the solar zenith angle is 0.15 and the surface albedo is zero in all figures in this paper. The results have been averaged over the azimuth angle ϕ measured from the incident plane over a range $0^\circ < \phi < 30^\circ$ on the left side of the figure and $150^\circ < \phi < 180^\circ$ on the right side. The solar horizon is on the left side of the figure, the nadir at the center, and the antisolar horizon on the right side. Results are given for the following models: (diamond and cross) single scattering from all aerosol and all Rayleigh atmosphere respectively; (plus, triangle, and octagon) single scattering from model earth's atmosphere with one-third, normal, and three times normal aerosol amount respectively; (solid circle, solid triangle with point up, and solid triangle with point down) multiple scattering from model earth's atmosphere with one-third, normal, and three times normal aerosol amount respectively; (solid square) multiple scattering from model earth's atmosphere with normal aerosol amount and with $\tau = 1$ nimbostratus cloud at 5 km altitude.

Fig. 2. Polarization of reflected radiation at $\lambda = 0.4\mu$ for $30^\circ < \phi < 60^\circ$ and $120^\circ < \phi < 150^\circ$.

Fig. 3. Polarization of reflected radiation at $\lambda = 0.4\mu$ for $60^\circ < \phi < 120^\circ$.

Fig. 4. Plane of polarization χ of reflected radiation as a function of μ at $\lambda = 0.4\mu$ for $0^\circ < \phi < 30^\circ$ and $150^\circ < \phi < 180^\circ$.

Fig. 5. Plane of polarization of reflected radiation at $\lambda = 0.4\mu$ for $30^\circ < \phi < 60^\circ$ and $120^\circ < \phi < 150^\circ$.

Fig. 6. Plane of polarization of reflected radiation at $\lambda = 0.4\mu$ for $60^\circ < \phi < 120^\circ$.

Fig. 7. Polarization of reflected radiation at $\lambda = 0.7\mu$ for $0^\circ < \phi < 30^\circ$ and $150^\circ < \phi < 180^\circ$.

Fig. 8. Polarization of reflected radiation at $\lambda = 0.7\mu$ for $30^\circ < \phi < 60^\circ$ and $120^\circ < \phi < 150^\circ$.

Fig. 9. Polarization of reflected radiation at $\lambda = 0.7\mu$ for $60^\circ < \phi < 120^\circ$.

Fig. 10. Plane of polarization of reflected radiation at $\lambda = 0.7\mu$ for $0^\circ < \phi < 30^\circ$ and $150^\circ < \phi < 180^\circ$.

Fig. 11. Plane of polarization of reflected radiation at $\lambda = 0.7\mu$ for $30^\circ < \phi < 60^\circ$ and $120^\circ < \phi < 150^\circ$.

Fig. 12. Plane of polarization of reflected radiation at $\lambda = 0.7\mu$ for $60^\circ < \phi < 120^\circ$.

Fig. 13. Polarization of transmitted radiation at $\lambda = 0.4\mu$ as a function of the zenith angle μ for $0^\circ < \phi < 30^\circ$ and $150^\circ < \phi < 180^\circ$. The cosine of the solar zenith angle is 0.15 and the surface albedo is zero in all figures in this paper. The solar horizon is on the left side of the figure, the zenith at the center, and the antisolar horizon on the right side. The direction of the unscattered solar photons is between the solar horizon and the zenith.

Fig. 14. Polarization of transmitted radiation at $\lambda = 0.4\mu$ for $30^\circ < \phi < 60^\circ$ and $120^\circ < \phi < 150^\circ$.

Fig. 15. Polarization of transmitted radiation at $\lambda = 0.4\mu$ for $60^\circ < \phi < 120^\circ$.

Fig. 16. Plane of polarization of transmitted radiation at $\lambda = 0.4\mu$ for $0^\circ < \phi < 30^\circ$ and $150^\circ < \phi < 180^\circ$.

Fig. 17. Plane of polarization of transmitted radiation at $\lambda = 0.4\mu$ for $30^\circ < \phi < 60^\circ$ and $120^\circ < \phi < 150^\circ$.

Fig. 18. Plane of polarization of transmitted radiation at $\lambda = 0.4\mu$ for $60^\circ < \phi < 120^\circ$.

Fig. 19. Polarization of transmitted radiation at $\lambda = 0.7\mu$ for $0^\circ < \phi < 30^\circ$ and $150^\circ < \phi < 180^\circ$.

Fig. 20. Polarization of transmitted radiation at $\lambda = 0.7\mu$ for $30^{\circ} < \phi < 60^{\circ}$ and $120^{\circ} < \phi < 150^{\circ}$.

Fig. 21. Polarization of transmitted radiation at $\lambda = 0.7\mu$ for $60^{\circ} < \phi < 120^{\circ}$.

Fig. 22. Plane of polarization of transmitted radiation at $\lambda = 0.7\mu$ for $0^{\circ} < \phi < 30^{\circ}$ and $150^{\circ} < \phi < 180^{\circ}$.

Fig. 23. Plane of polarization of transmitted radiation at $\lambda = 0.7\mu$ for $30^{\circ} < \phi < 60^{\circ}$ and $120^{\circ} < \phi < 150^{\circ}$.

Fig. 24. Plane of polarization of transmitted radiation at $\lambda = 0.7\mu$ for $60^{\circ} < \phi < 120^{\circ}$.

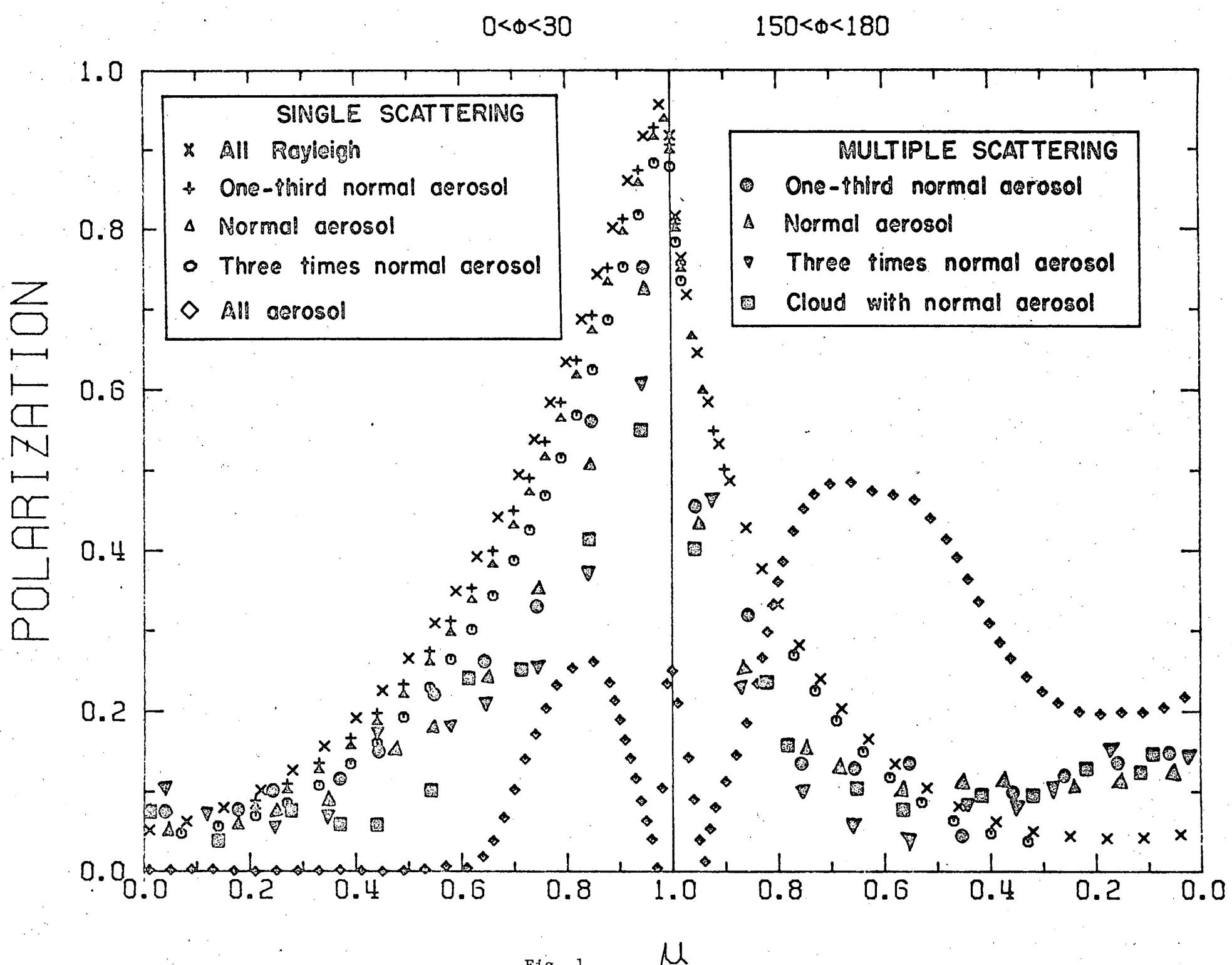
0<Φ<30
150<Φ<180
SINGLE SCATTERING
All Rayleigh
One-third normal aerosol
Normal aerosol
Three times normal aerosol
All aerosol
MULTIPLE SCATTERING
One-third normal aerosol
Normal aerosol
Three times normal aerosol
Cloud with normal aerosol
POLARIZATION
1.0
0.8
0.6
0.4
0.2
0.0
0.0
0.2
0.4
0.6
0.8
1.0
0.8
0.6
0.4
0.2
0.0
μ

Fig. 1

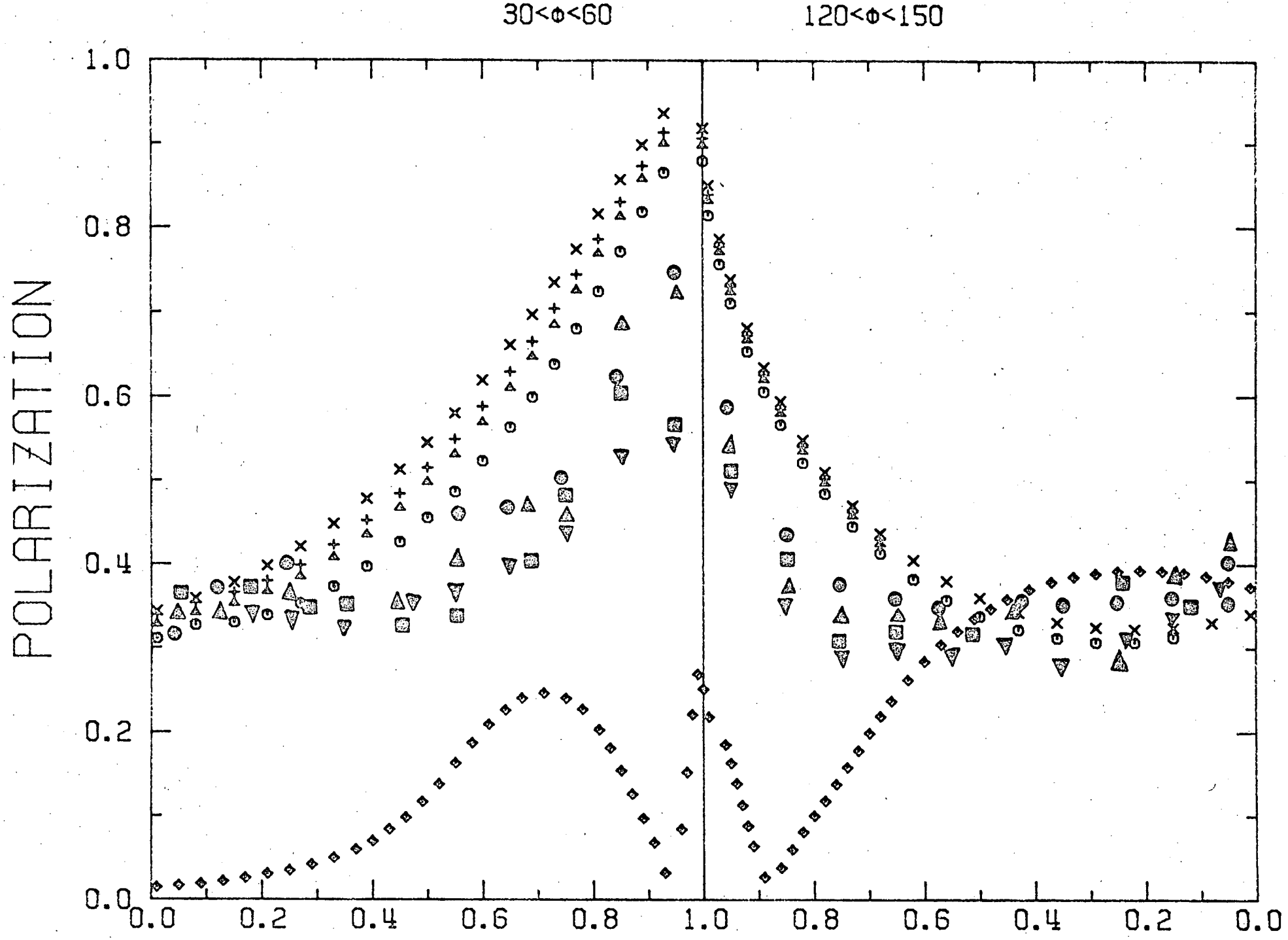
30<Φ<60
120<Φ<150
POLARIZATION
1.0
0.8
0.6
0.4
0.2
0.0
0.0
0.2
0.4
0.6
0.8
1.0
0.8
0.6
0.4
0.2
0.0

Fig. 2

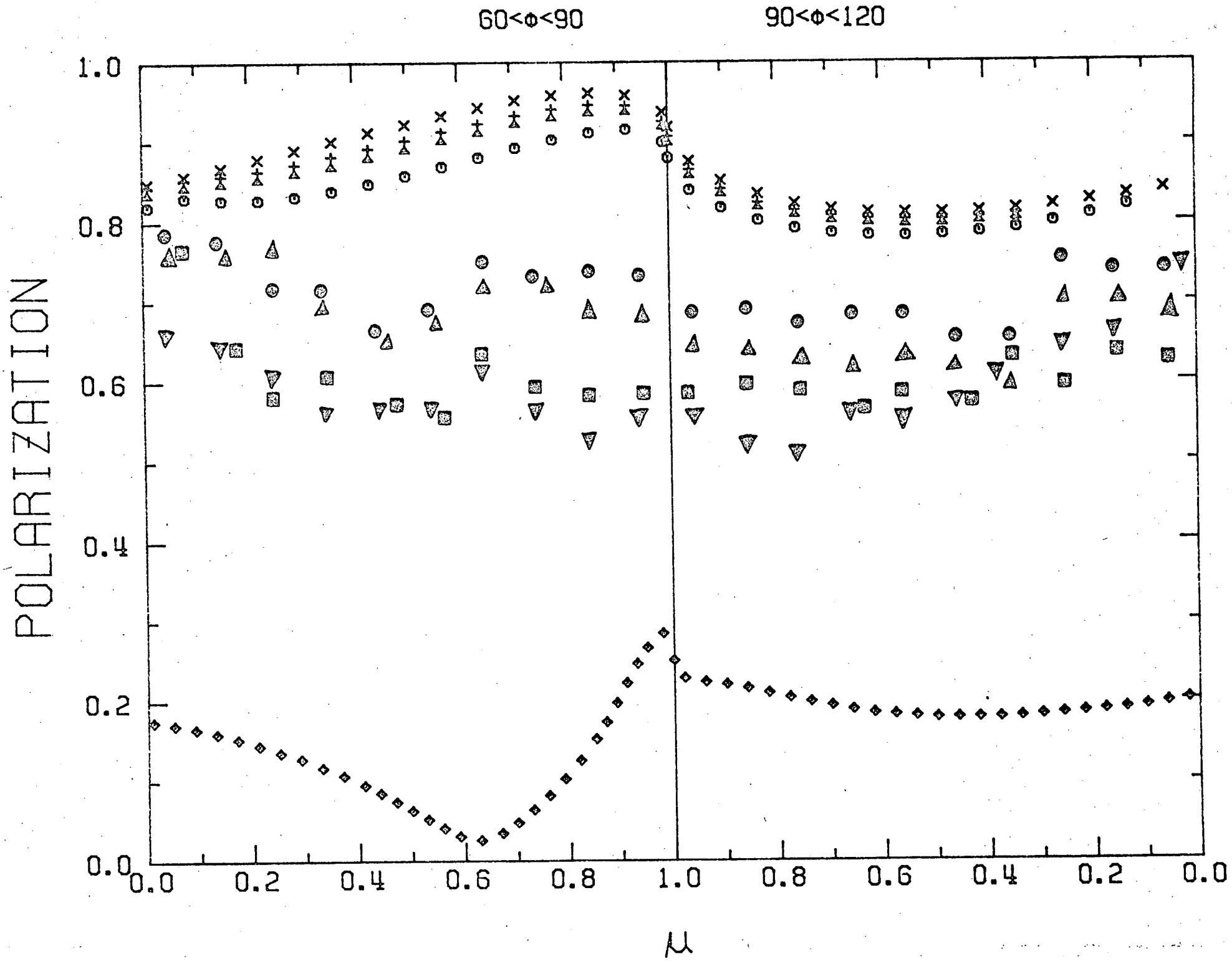
60<Φ<90
90<Φ<120
POLARIZATION
1.0
0.8
0.6
0.4
0.2
0.0
0.0
0.2
0.4
0.6
0.8
1.0
0.8
0.6
0.4
0.2
0.0
μ

Fig. 3

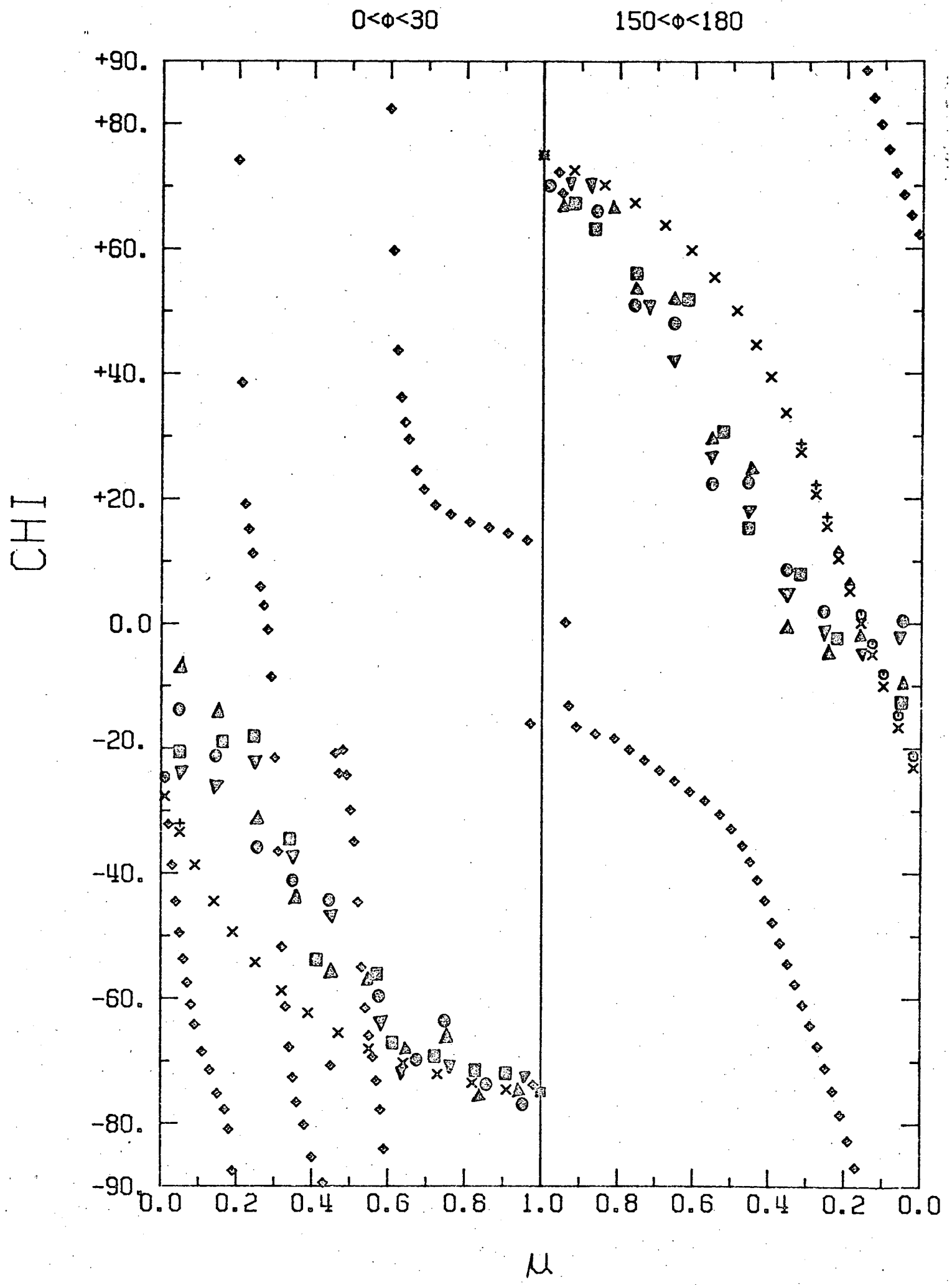
0<φ<30
150<φ<180
+90.
+80.
+60.
+40.
+20.
0.0
-20.
-40.
-60.
-80.
-90.
CHI
0.0
0.2
0.4
0.6
0.8
1.0
0.8
0.6
0.4
0.2
0.0
μ

Fig. 4

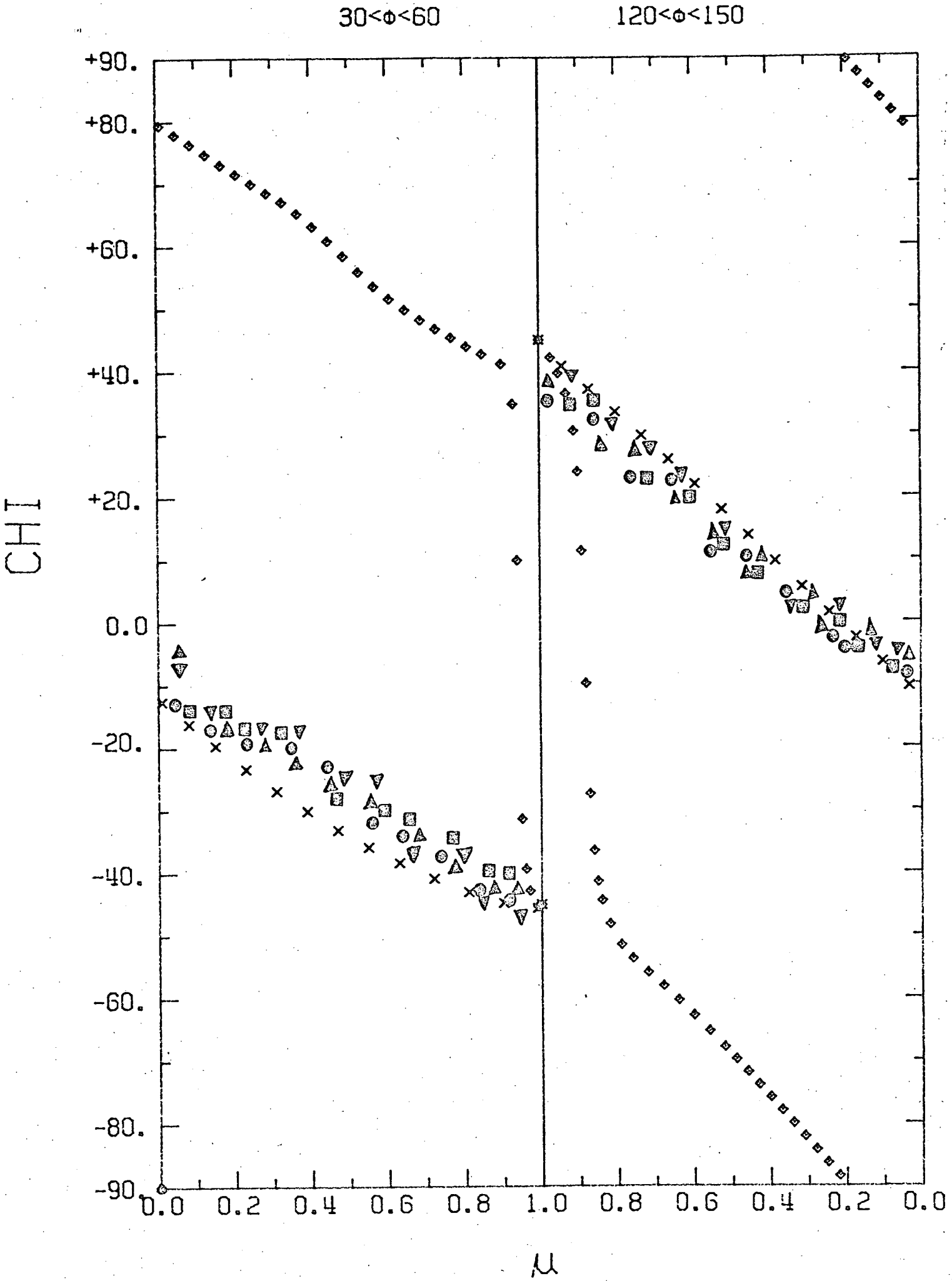
30<Φ<60
120<Φ<150
+90.
+80.
+60.
+40.
+20.
0.0
-20.
-40.
-60.
-80.
-90.
CHI
0.0
0.2
0.4
0.6
0.8
1.0
0.8
0.6
0.4
0.2
0.0
μ

Fig. 5

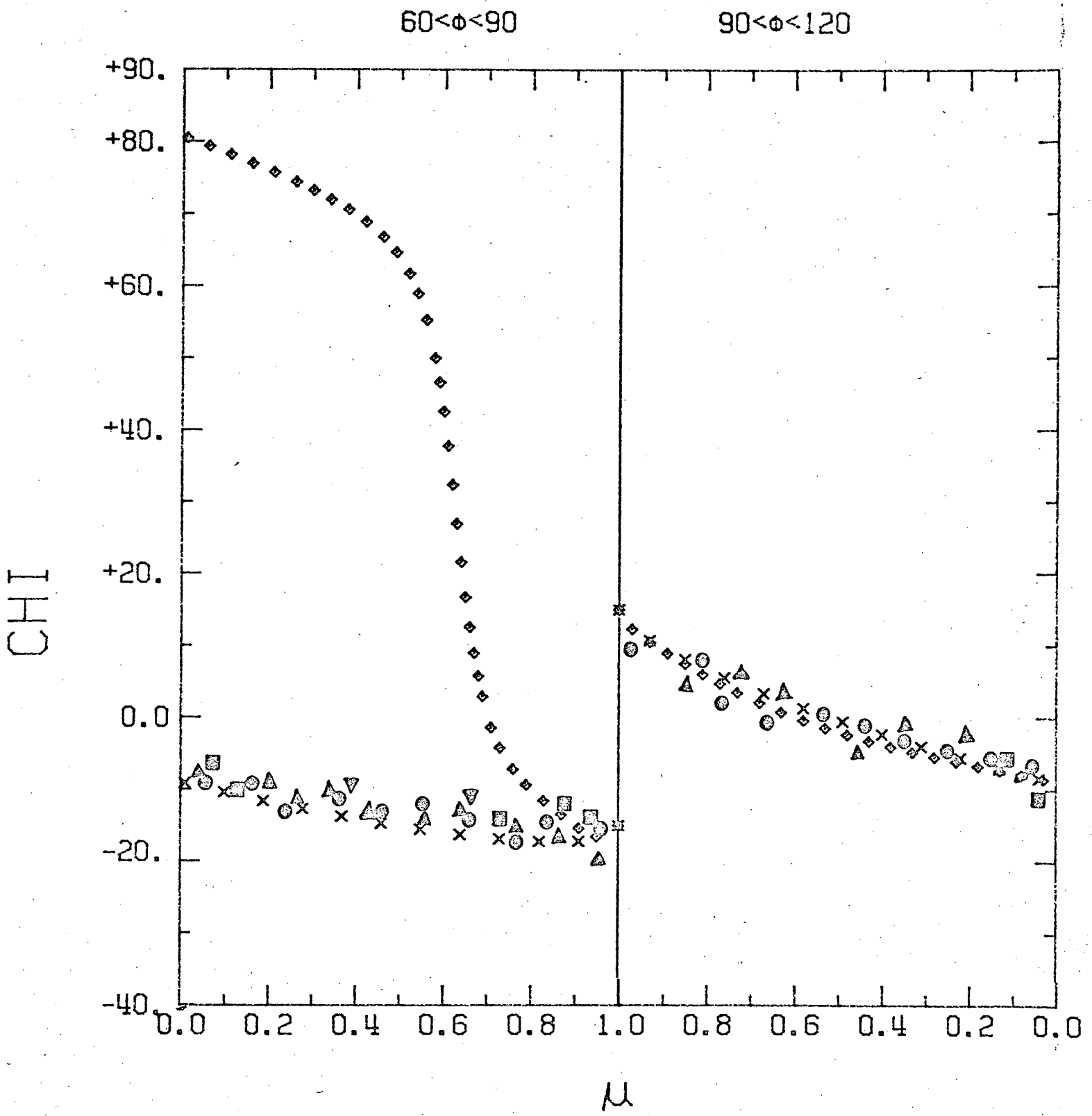
60<Φ<90
90<Φ<120
+90.
+80.
+60.
+40.
+20.
0.0
-20.
-40.
0.0
0.2
0.4
0.6
0.8
1.0
0.8
0.6
0.4
0.2
0.0
CHI
μ

Fig. 6

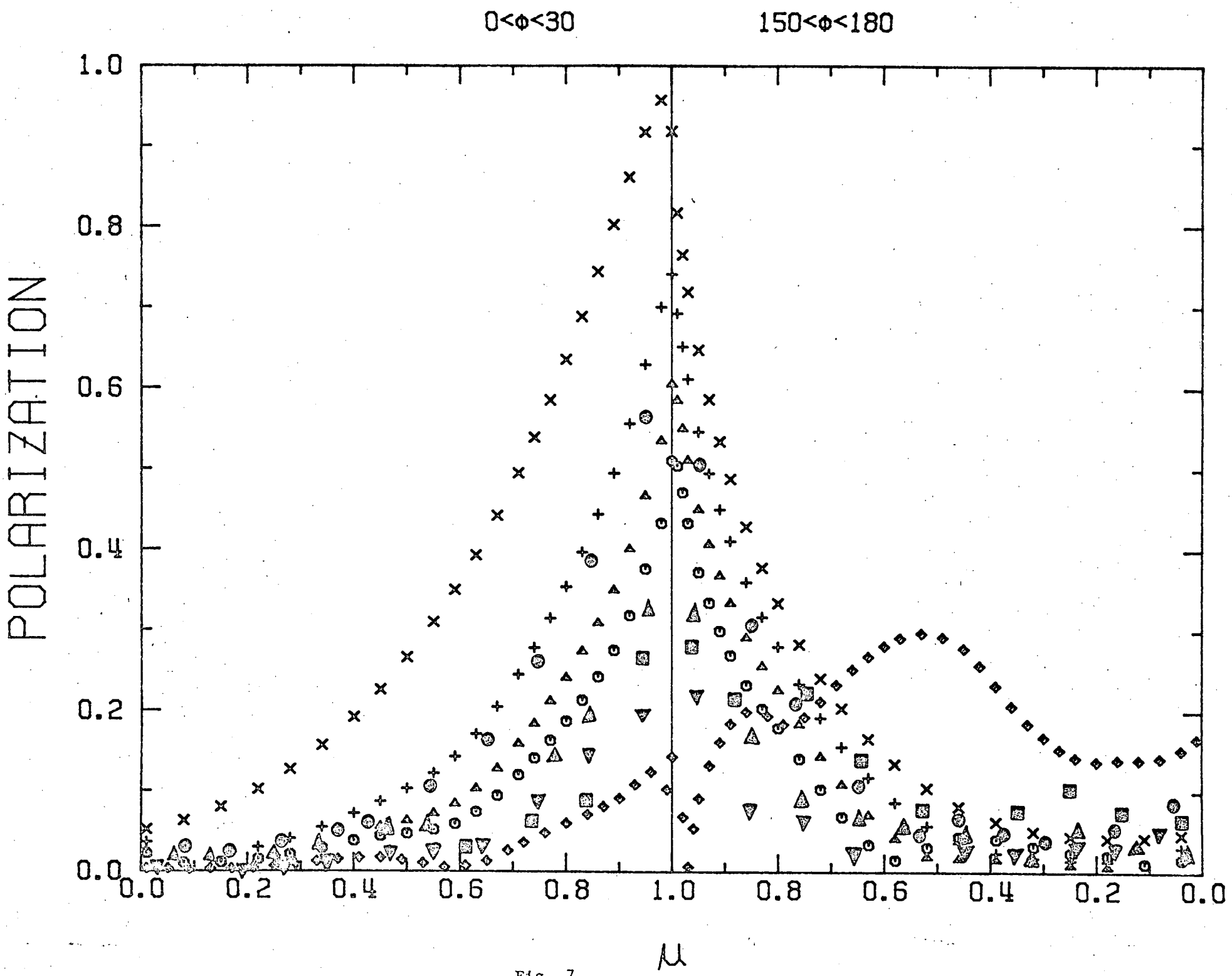
0<φ<30
150<φ<180
POLARIZATION
1.0
0.8
0.6
0.4
0.2
0.0
0.0
0.2
0.4
0.6
0.8
1.0
0.8
0.6
0.4
0.2
0.0
μ

Fig. 7

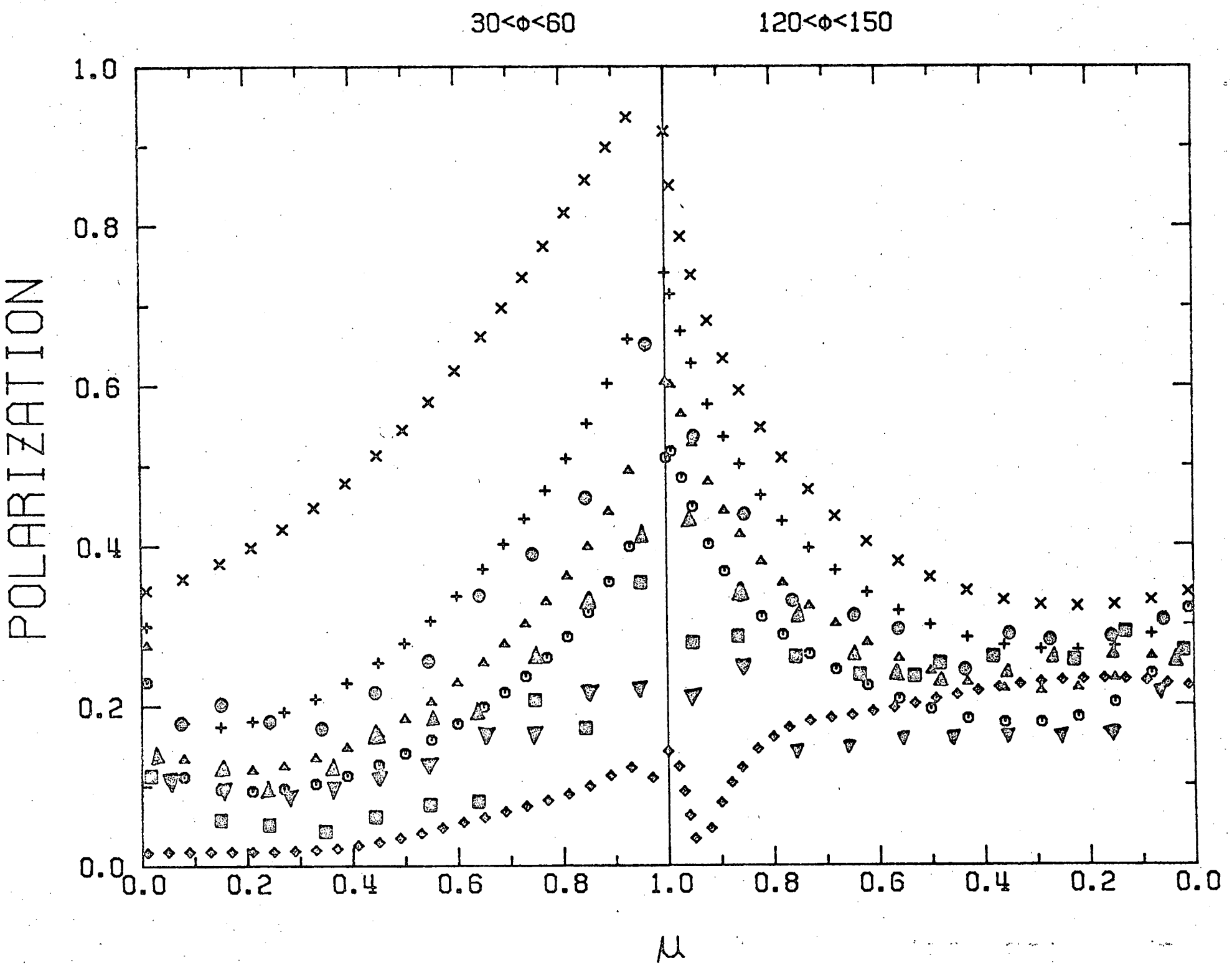
30<φ<60
120<φ<150
POLARIZATION
1.0
0.8
0.6
0.4
0.2
0.0
0.0
0.2
0.4
0.6
0.8
1.0
0.8
0.6
0.4
0.2
0.0
μ

Fig. 8

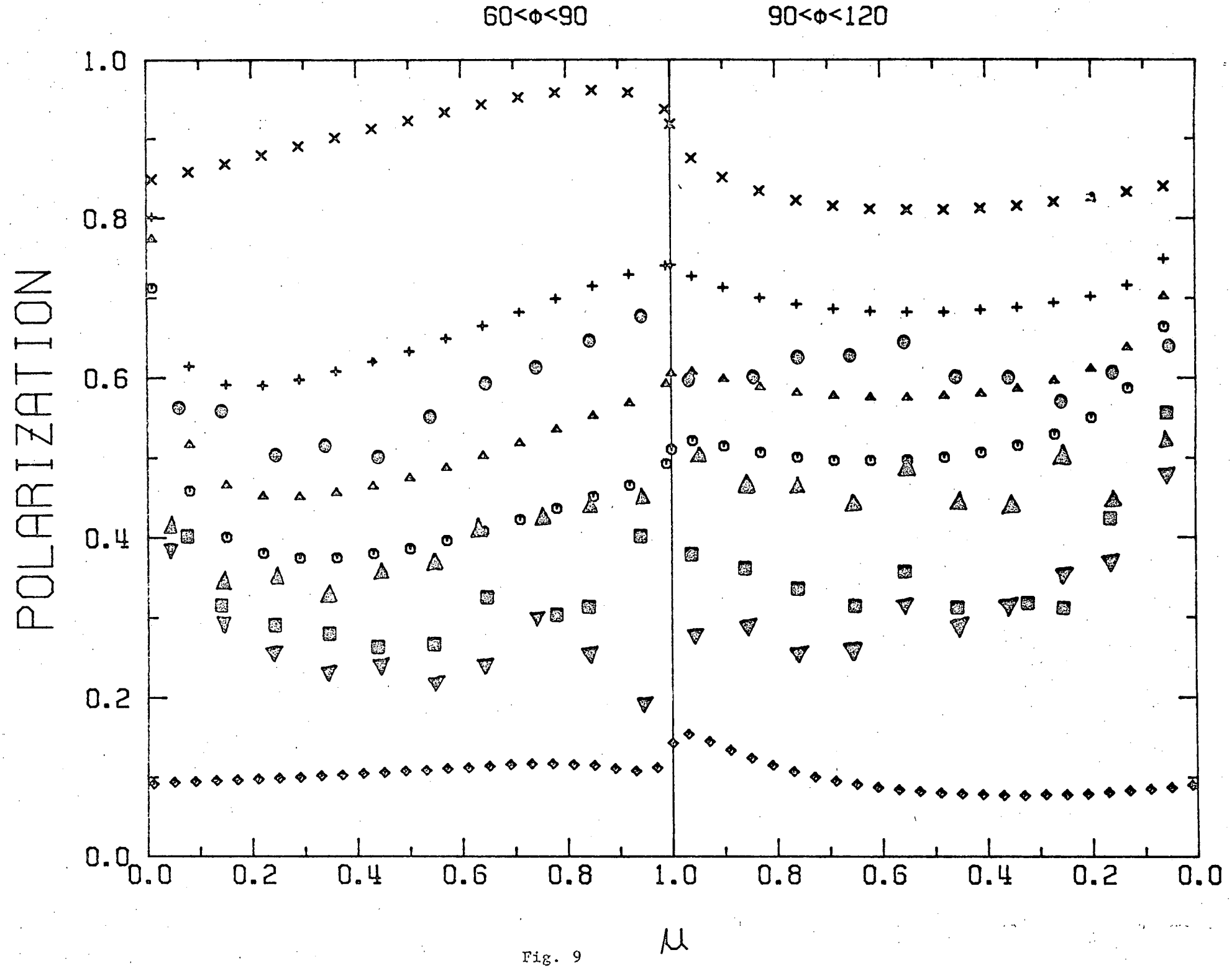
60<φ<90
90<φ<120
POLARIZATION
1.0
0.8
0.6
0.4
0.2
0.0
0.0
0.2
0.4
0.6
0.8
1.0
0.8
0.6
0.4
0.2
0.0
μ

Fig. 9

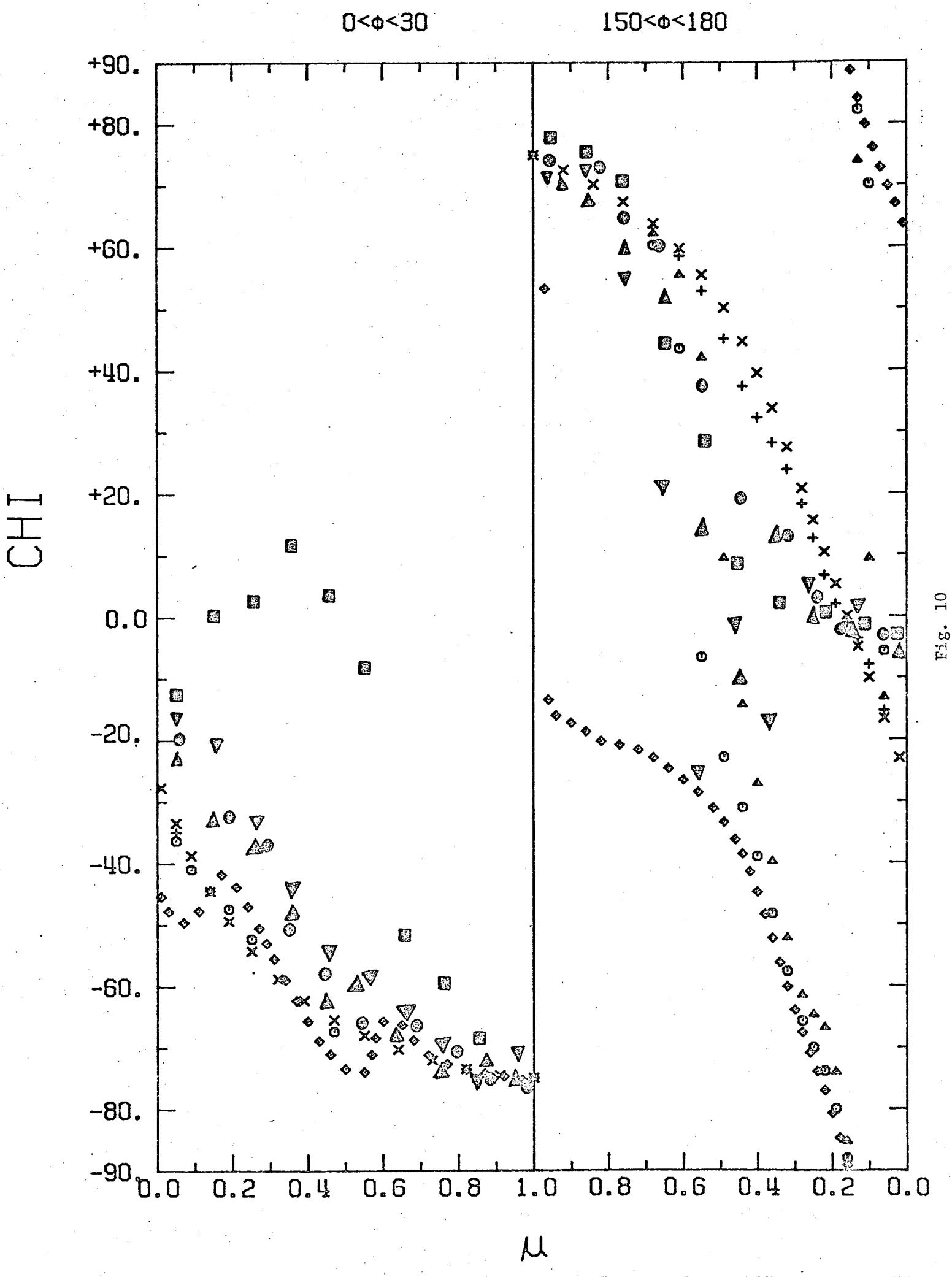
0<φ<30
150<φ<180
+90.
+80.
+60.
+40.
+20.
0.0
-20.
-40.
-60.
-80.
-90.
CHI
0.0
0.2
0.4
0.6
0.8
1.0
0.8
0.6
0.4
0.2
0.0
μ

Fig. 10

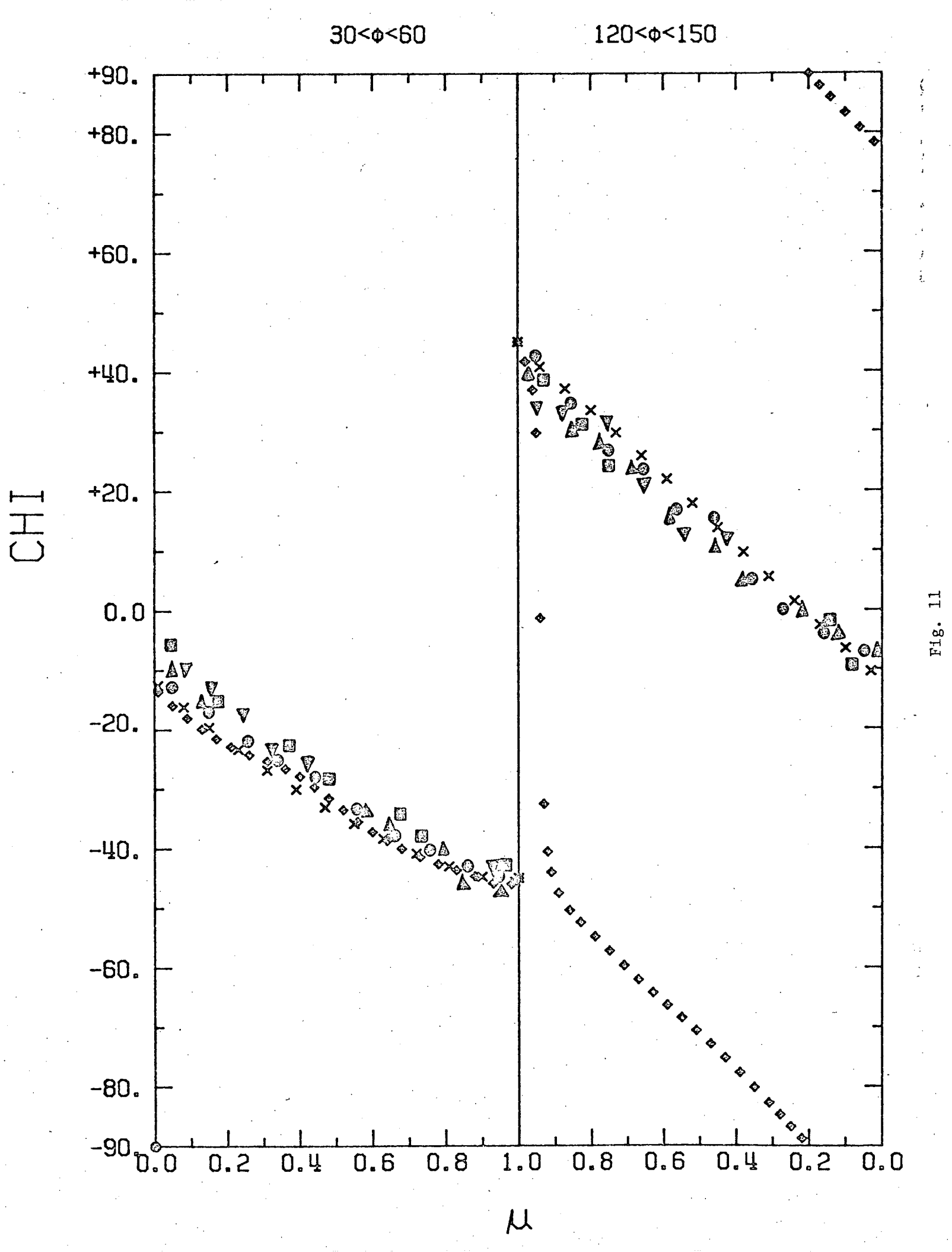
30<φ<60
120<φ<150
+90.
+80.
+60.
+40.
+20.
0.0
-20.
-40.
-60.
-80.
-90.
CHI
0.0
0.2
0.4
0.6
0.8
1.0
0.8
0.6
0.4
0.2
0.0
μ

Fig. 11

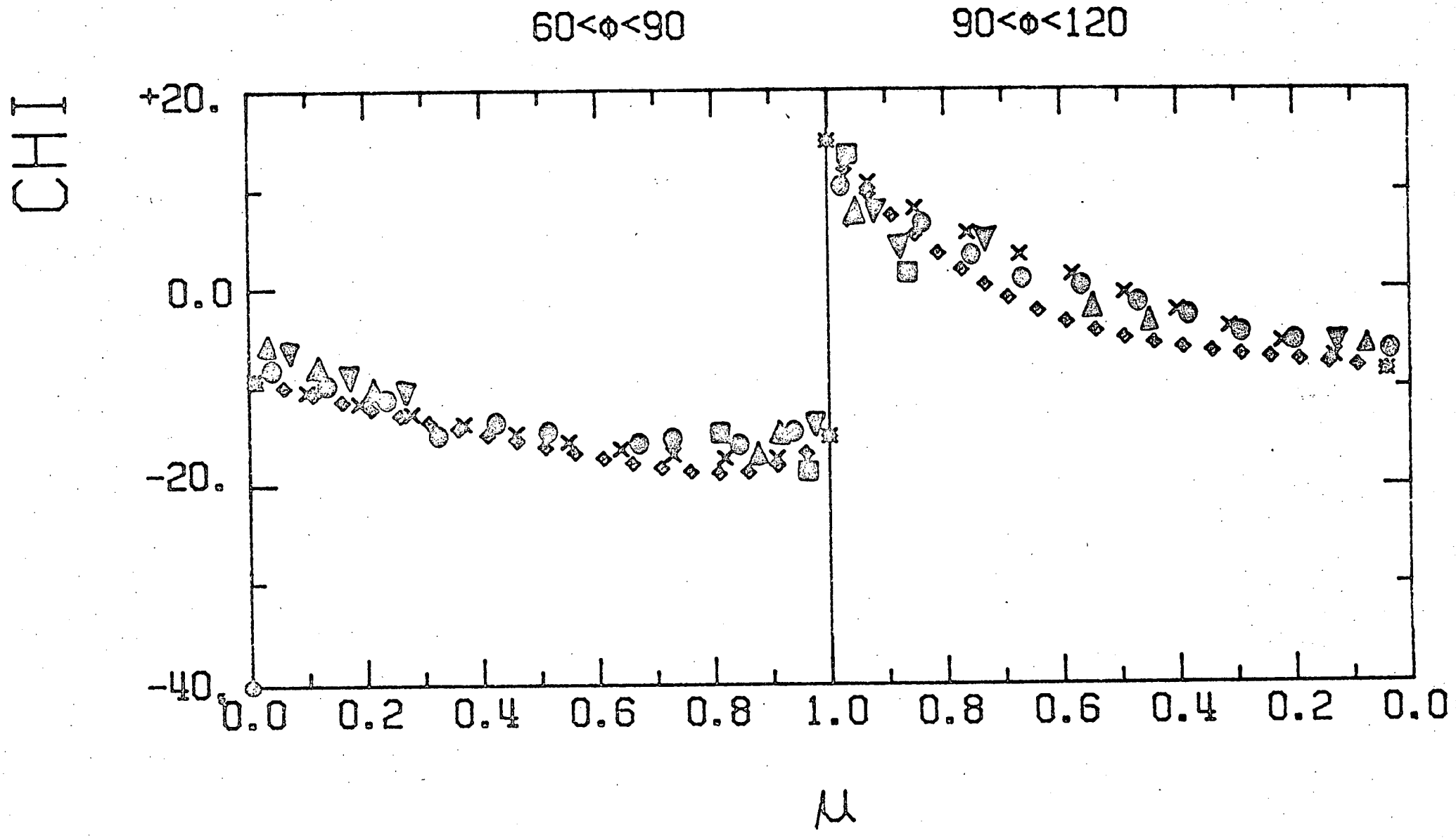

Fig. 12

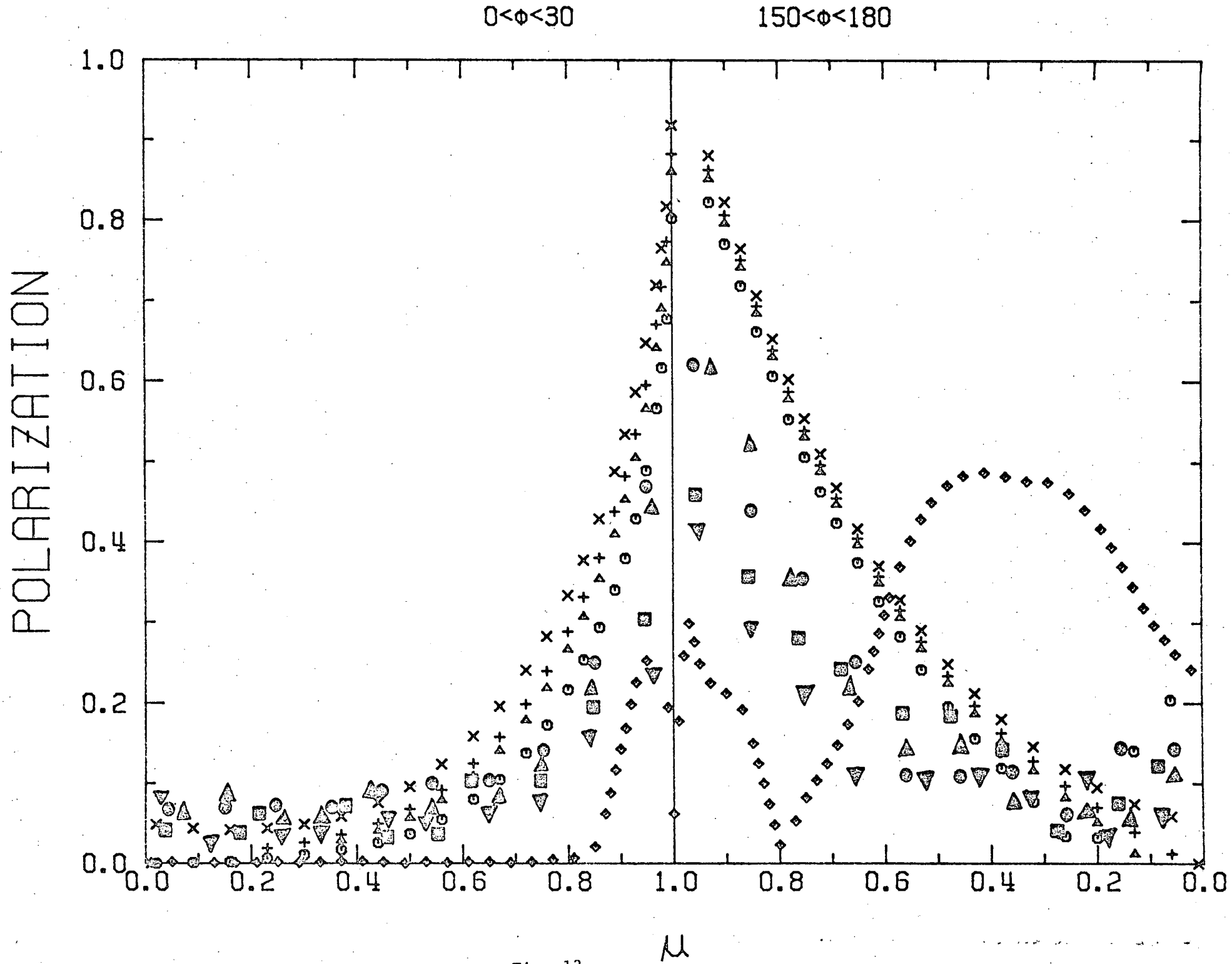
0<φ<30
150<φ<180
POLARIZATION
1.0
0.8
0.6
0.4
0.2
0.0
0.0
0.2
0.4
0.6
0.8
1.0
0.8
0.6
0.4
0.2
0.0
μ

Fig. 13

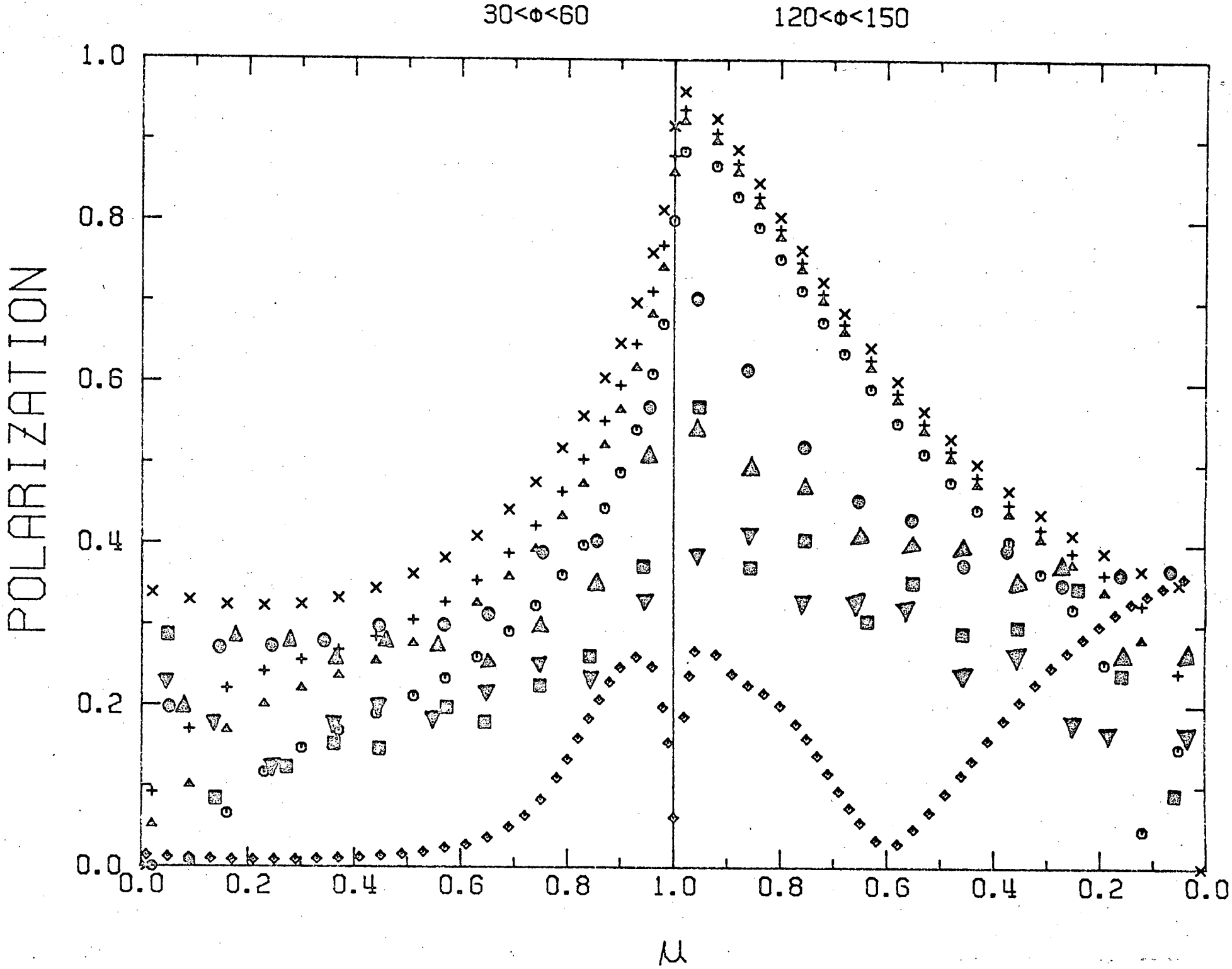
30<Φ<60
120<Φ<150
POLARIZATION
1.0
0.8
0.6
0.4
0.2
0.0
0.0
0.2
0.4
0.6
0.8
1.0
0.8
0.6
0.4
0.2
0.0
μ

Fig. 14

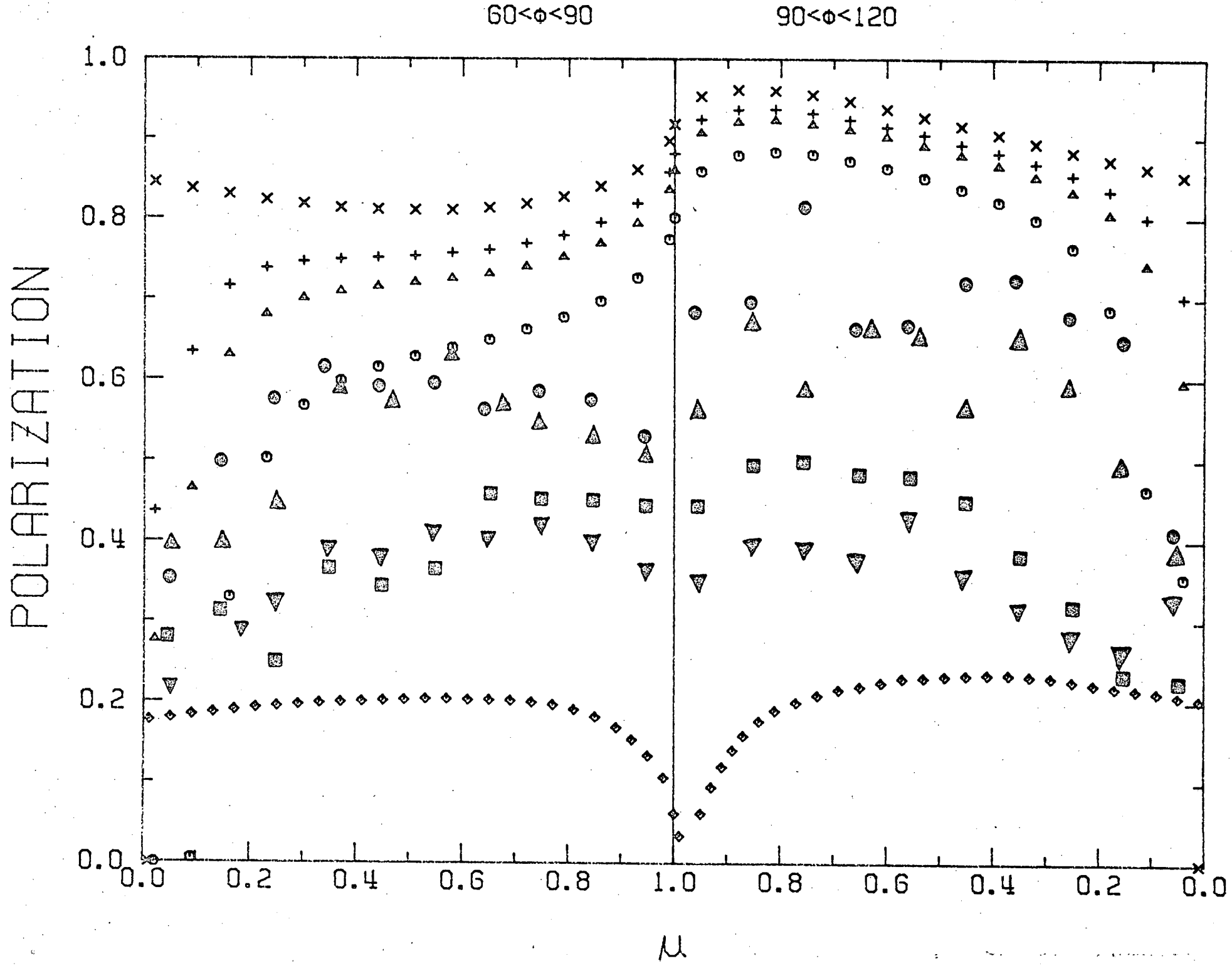
60<Φ<90
90<Φ<120
POLARIZATION
1.0
0.8
0.6
0.4
0.2
0.0
0.0
0.2
0.4
0.6
0.8
1.0
0.8
0.6
0.4
0.2
0.0
μ

Fig. 15

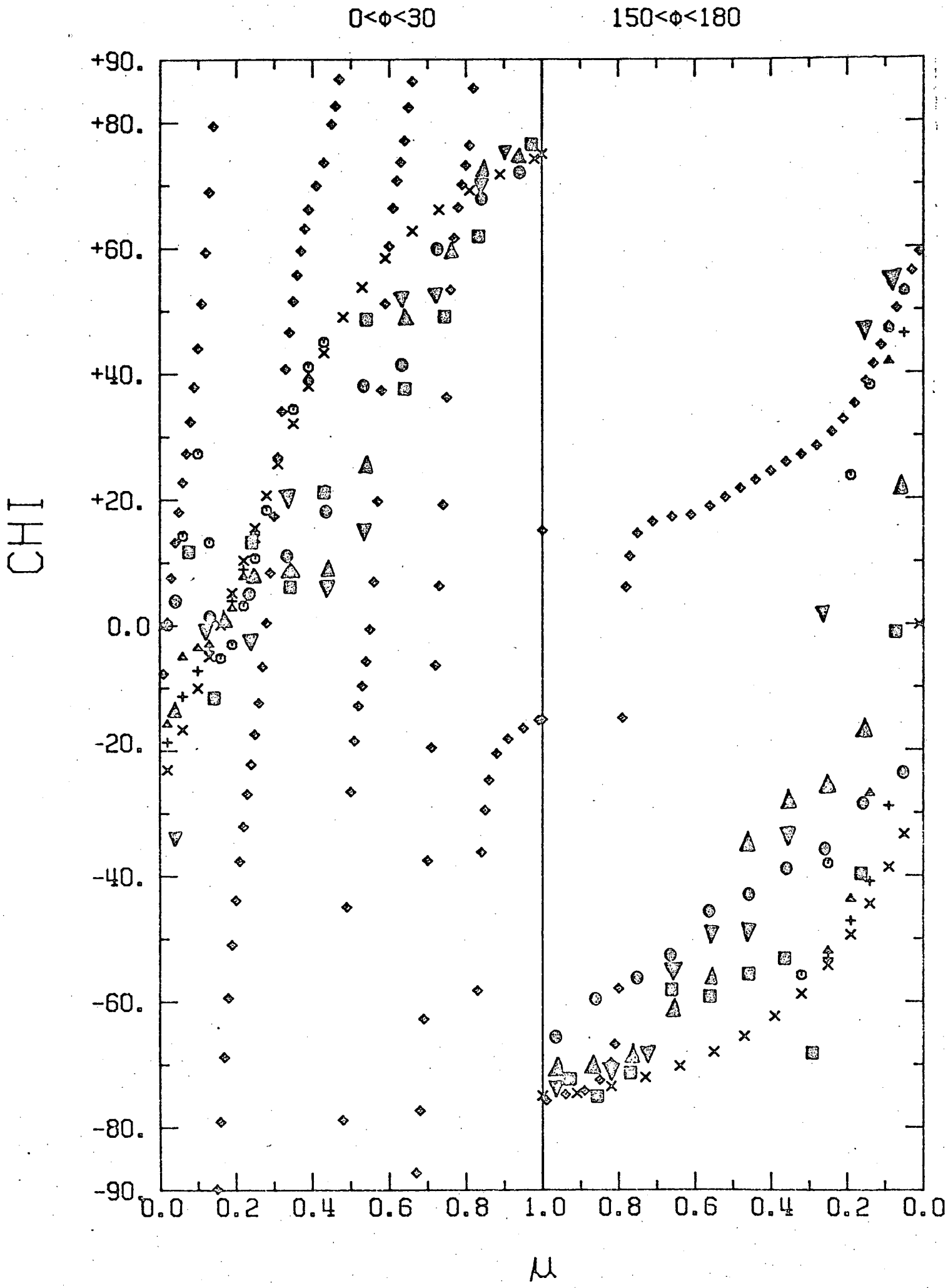
0<φ<30
150<φ<180
+90.
+80.
+60.
+40.
+20.
0.0
-20.
-40.
-60.
-80.
-90.
CHI
0.0
0.2
0.4
0.6
0.8
1.0
0.8
0.6
0.4
0.2
0.0
μ

Fig. 16

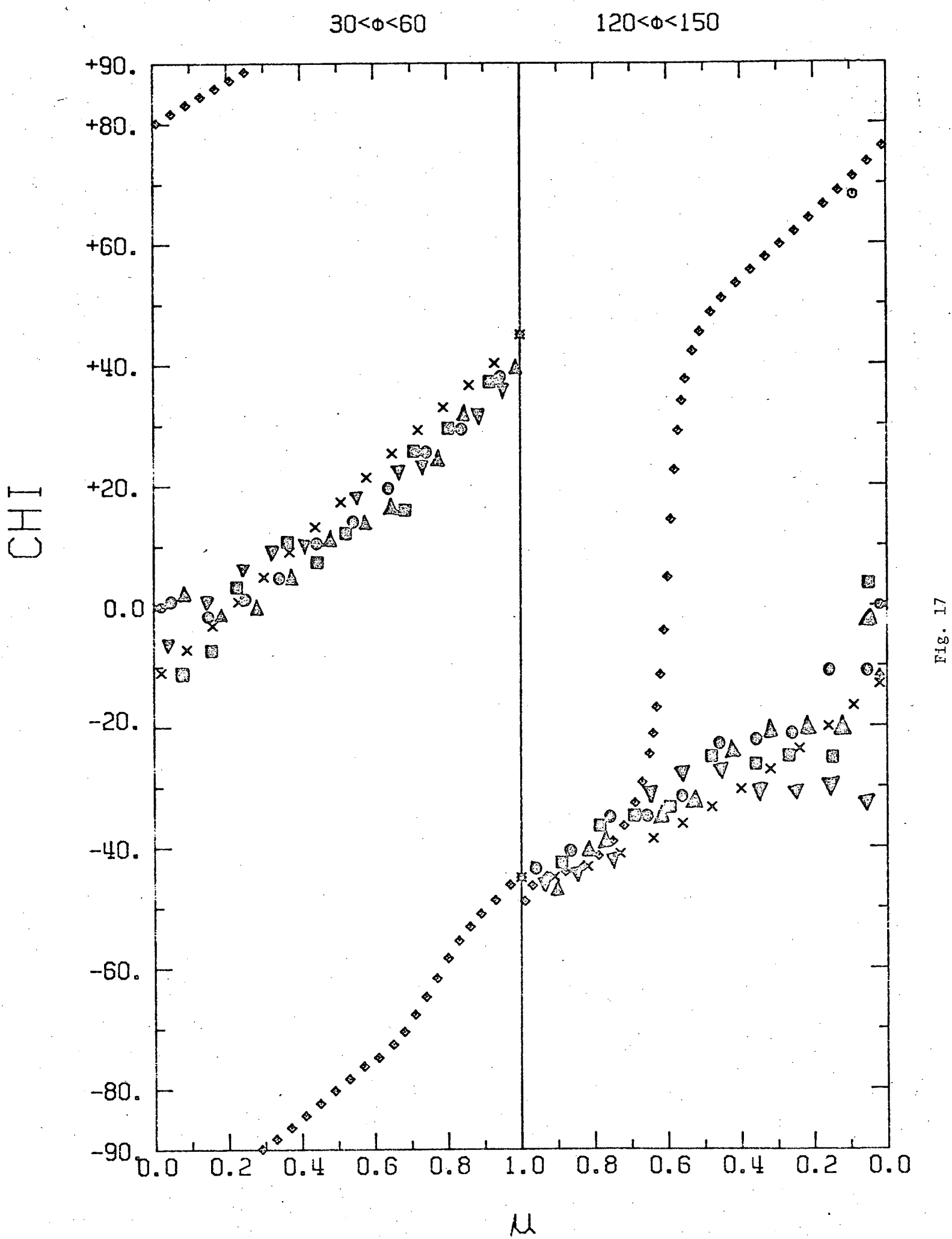
30<Φ<60
120<Φ<150
+90.
+80.
+60.
+40.
+20.
0.0
-20.
-40.
-60.
-80.
-90.
CHI
0.0
0.2
0.4
0.6
0.8
1.0
0.8
0.6
0.4
0.2
0.0
μ

Fig. 17

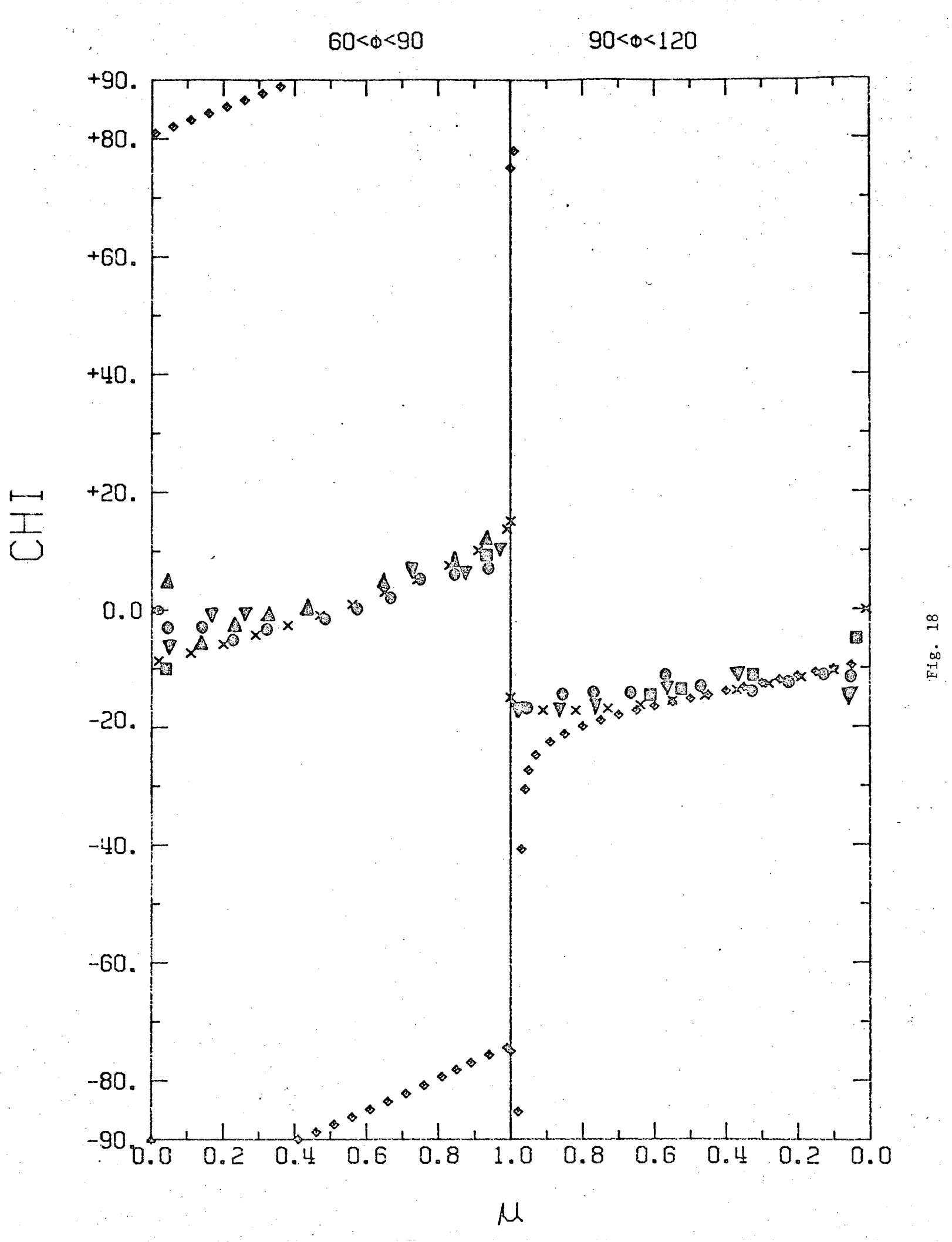
60<Φ<90
90<Φ<120
+90.
+80.
+60.
+40.
+20.
0.0
-20.
-40.
-60.
-80.
-90.
CHI
0.0
0.2
0.4
0.6
0.8
1.0
0.8
0.6
0.4
0.2
0.0
μ

Fig. 18

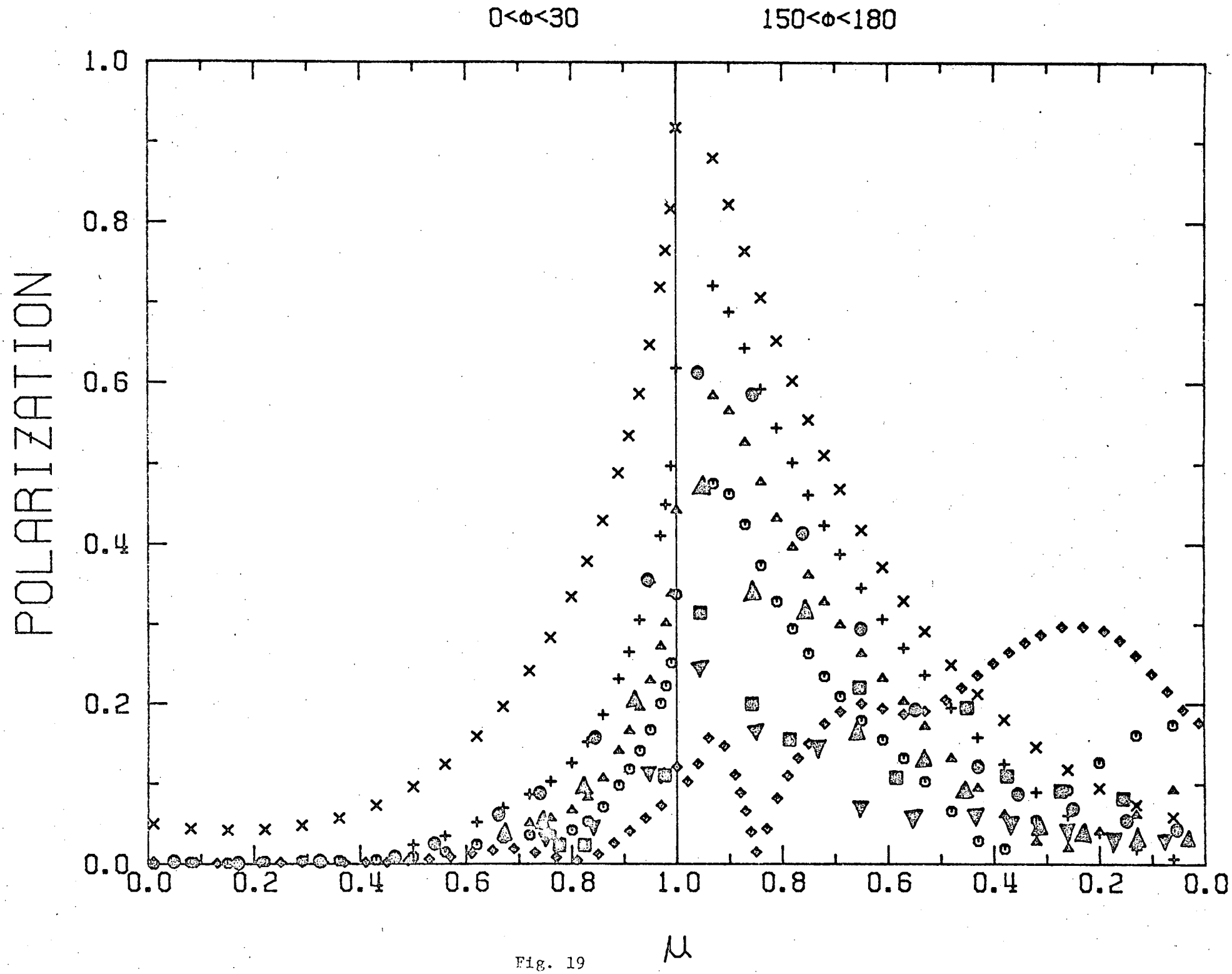
0<φ<30
150<φ<180
POLARIZATION
1.0
0.8
0.6
0.4
0.2
0.0
0.0
0.2
0.4
0.6
0.8
1.0
0.8
0.6
0.4
0.2
0.0
μ

Fig. 19

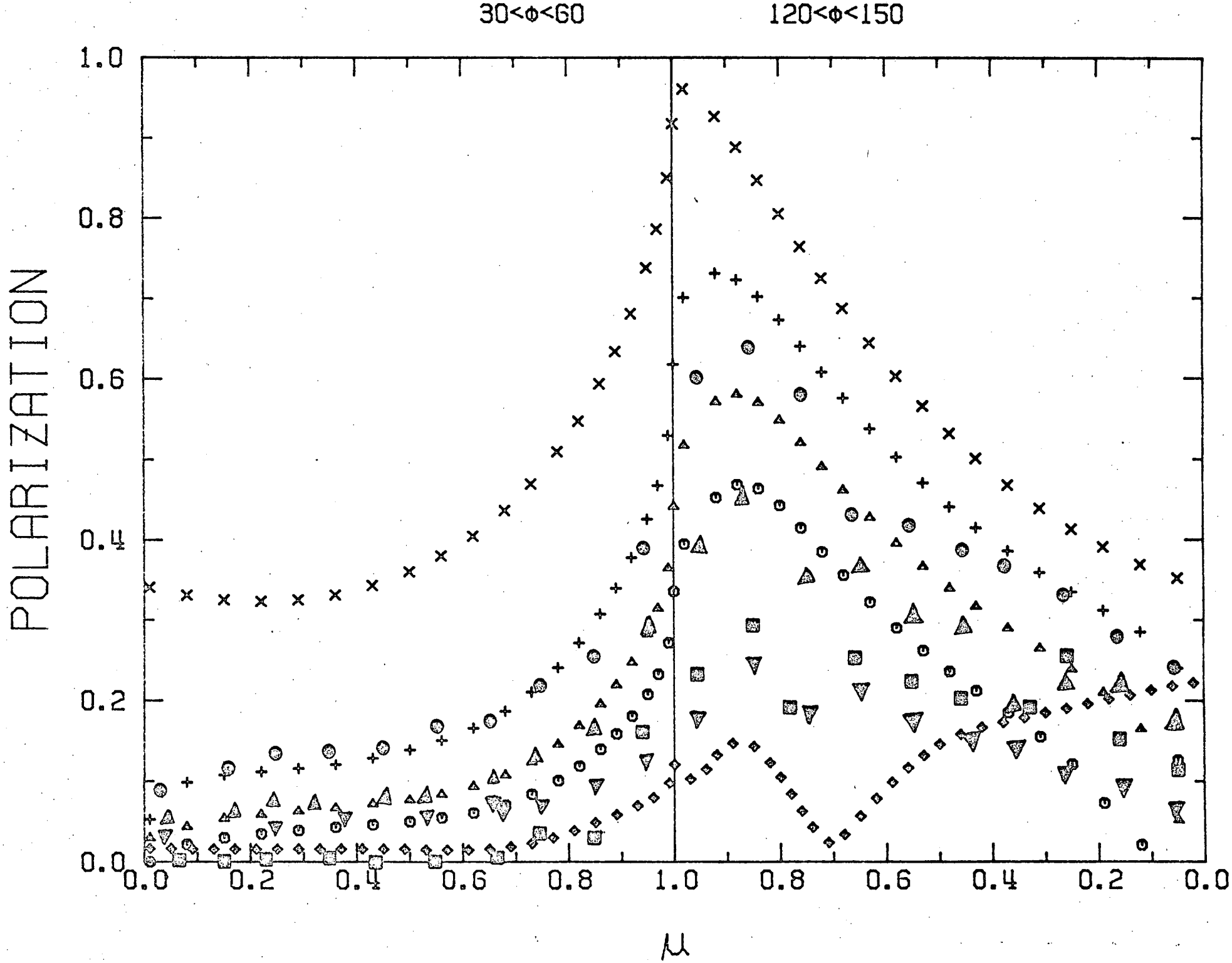
30<φ<60
120<φ<150
POLARIZATION
1.0
0.8
0.6
0.4
0.2
0.0
0.0
0.2
0.4
0.6
0.8
1.0
0.8
0.6
0.4
0.2
0.0
μ

Fig. 20

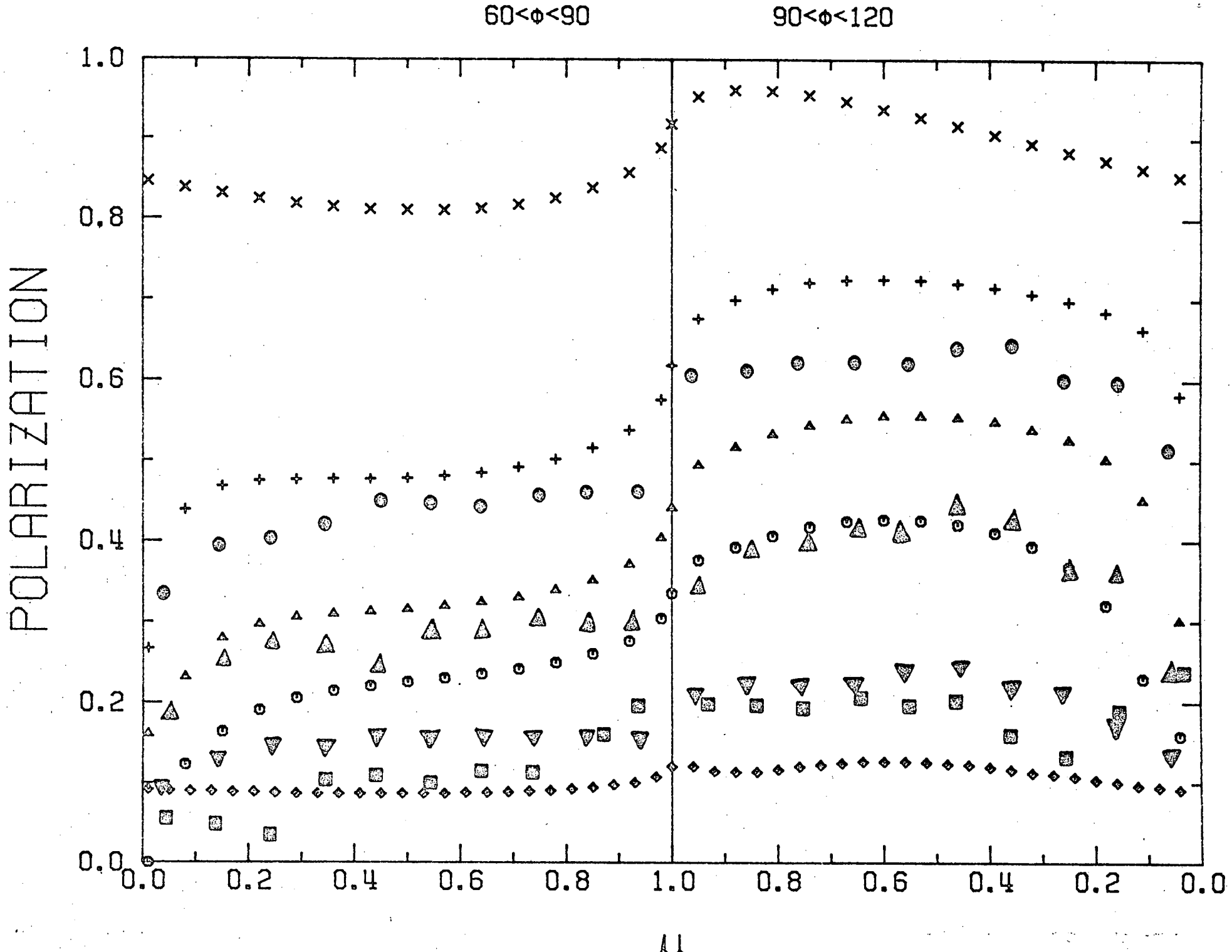
60<φ<90
90<φ<120
POLARIZATION
1.0
0.8
0.6
0.4
0.2
0.0
0.0
0.2
0.4
0.6
0.8
1.0
0.8
0.6
0.4
0.2
0.0
μ

Fig. 21

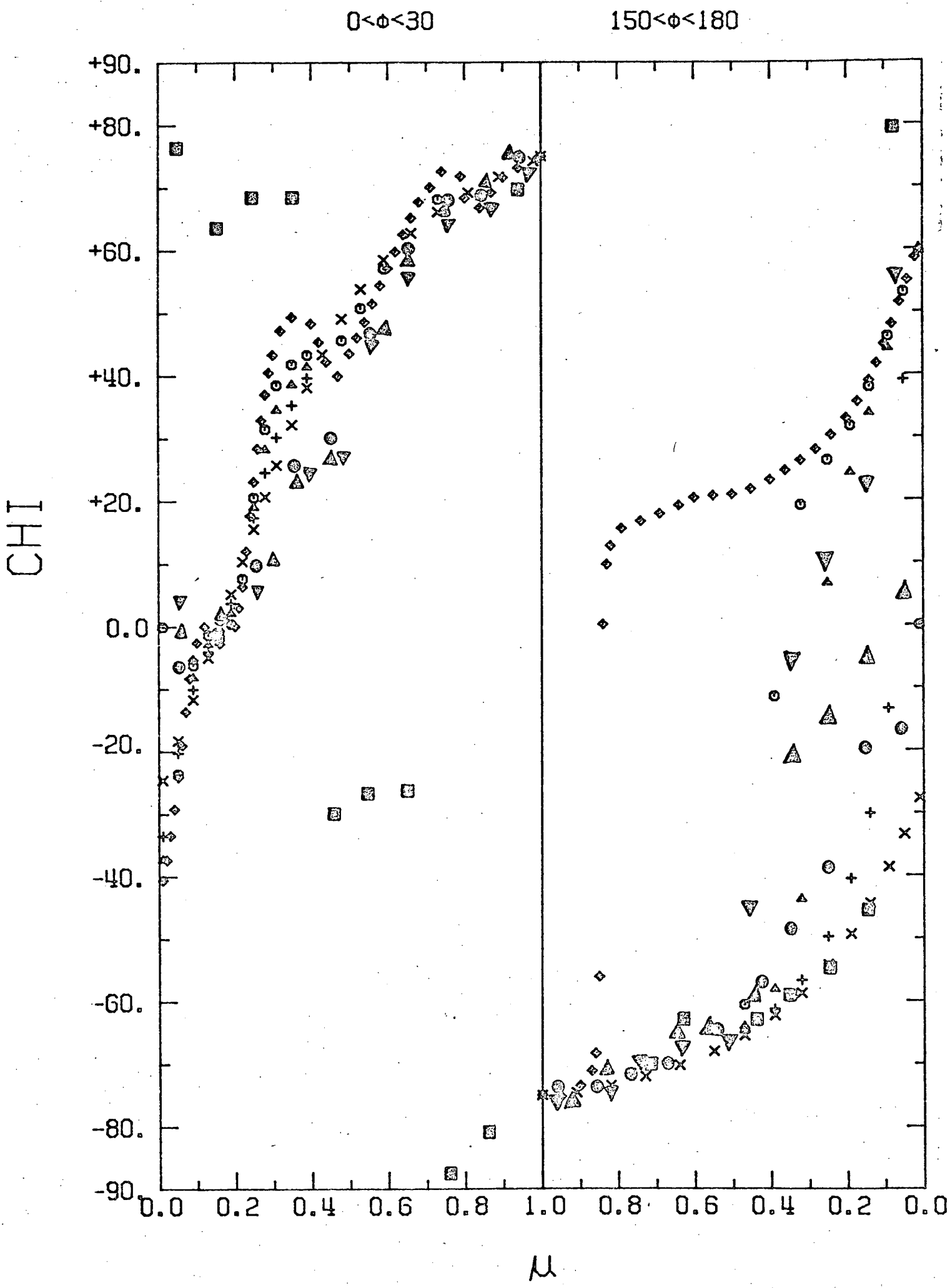
0<φ<30
150<φ<180
+90.
+80.
+60.
+40.
+20.
0.0
-20.
-40.
-60.
-80.
-90.
CHI
0.0
0.2
0.4
0.6
0.8
1.0
0.8
0.6
0.4
0.2
0.0
μ

Fig. 22

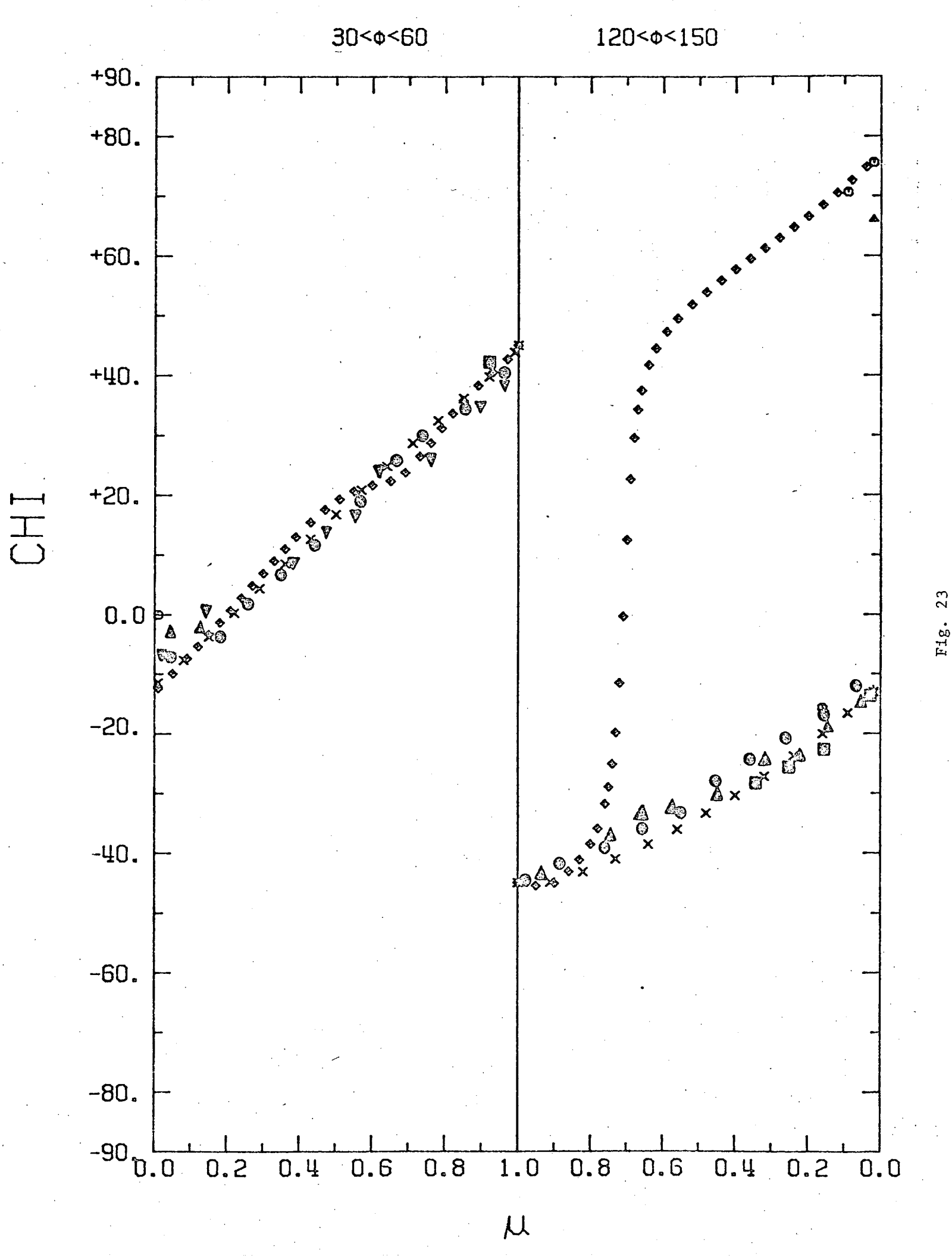
30<φ<60
120<φ<150
+90.
+80.
+60.
+40.
+20.
0.0
-20.
-40.
-60.
-80.
-90.
CHI
0.0
0.2
0.4
0.6
0.8
1.0
0.8
0.6
0.4
0.2
0.0
μ

Fig. 23